# The effect of the sampling frequency of a digital controller on the open loop frequency response function of a controlled system

# The Effect of the Sampling Frequency of a Digital Controller on the Open Loop Frequency Response Function of a Controlled System

Rudy Oosterbosch

DCT 2004.119

Traineeship report

Coach: P.W.J.M. Nuij

Technische Universiteit Eindhoven
Department of Mechanical Engineering
Dynamics and Control Technology Group

Eindhoven, December 2004

# Abstract

Many control systems use a digital controller to control a physical system. All these digital controllers are operating on a limiting number of samples. The digital character of the controller results in a periodicity of the control characteristic on multiples of the sampling frequency. Furthermore closed loop frequency components above the Nyquist frequency will be folded back (aliasing). In this report the influence of the sampling frequency of a digital controller is investigated for a fourth order system and the results are demonstrated on the open loop frequency response function. It is concluded that the sampling frequency certainly affects the open loop. To give a basis to the results the sampling frequency dependency of every component of the digital control system is examined separately.

# Contents

# Chapter 1

# Introduction

These days more and more digital computers are used to control physical systems. The most important reason for using a digital computer in control systems is the freedom and flexibility in the design of control algorithms. Typically for a digital system is that it is not continuous in time and also not continuous in amplitude. These two phenomena are directly related to respectively the sampling frequency and quantization. In other words in a digital control system the sampled amplitude is divided into equal parts by uniform quantization.

When analyzing digital control systems the effects of the sampling frequency and quantization should be taken into account. When these two effects are sufficiently small the digital control system equals almost a continuous equivalent. In theory this situation is very attractive but from an economical point of view high resolution and fast sampling computers are far from ideal. In this report only the effects of the sampling frequency are investigated and especially the effects of the sampling frequency on the open loop Frequency Response Function (FRF) of the controlled system. The open loop FRF is chosen here to investigate the effects because of its important role in the dynamic control. For instance the open loop FRF is often used for stability analysis.

To investigate the effects of the sampling frequency on the open loop FRF first in chapter 2 the procedure of identifying a general system with a frequency domain approach will be discussed. In chapter 3 a description is given of the considered system and how to identify this system. Next in chapter 4 two methods are discussed measuring the open loop FRF of the concerned system. Then in chapter 5 the results of the open loop FRF measurements are given. In this chapter also the sampling frequency dependency of the open loop FRF will be analyzed. In a try to explain the obtained results in chapter 6 the digital control system, with its specific components, is discussed in more detail, and in chapter 7 the sampling frequency dependency of each component is discussed separately. Finally in chapter 8 conclusions are drawn.

# Chapter 2

# System Identification

First a stable, linear, time invariant system with one excitation signal $x(t)$ and one response signal $y(t)$, as shown in figure 2.1, is considered. The observed system is assumed noise free. The question is how to estimate an input-output relation by measuring only the input and output. Here only a review about system identification is given more information can be found in .

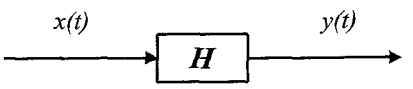


Figure 2.1: Single input single output System

## 2.1 Frequency Domain Approach

The relation between input and output can be described by a FRF. In this section the FRF is obtained using a frequency domain approach.

### 2.1.1 System Estimators

Estimates for obtaining the FRF are given by the so called $H_1(f)$ and $H_2(f)$ estimator [1]. These two estimators make use of power spectral density functions and they are defined by respectively

$$H_1(f) = \frac{S_{xy}(f)}{S_{xx}(f)} \tag{2.1}$$

$$H_2(f) = \frac{S_{yy}(f)}{S_{yx}(f)} \tag{2.2}$$

Here $S_{xx}(f)$ and $S_{yy}(f)$ are the auto spectral density functions of the respectively input signal $x(t)$ and output signal $y(t)$ and $S_{xy}(f)$ and $S_{yx}(f)$ are cross spectral density functions of input and output signal.

### 2.1.2 Power Spectral Density Functions

The auto spectral density function (also called auto power spectrum) gives information about the frequencies present in a signal and the contribution of each frequency component to the total power in the signal. The auto spectral density function for general stationary random data $x(t)$ for $-\infty < f < \infty$ is defined by

$$S_{xx}(f) = \lim_{T\to\infty} E\left[\hat{S}_{xx}(f,T)\right] \tag{2.3}$$

where $E\left[\hat{S}_{xx}(f,T)\right]$ is the expected value operation of the power spectral density estimate over the range $0 \leq t \leq T$. The power spectral density estimate is defined by

$$\hat{S}_{xx}(f,T) = \frac{1}{T}X^*(f,T)X(f,T) \tag{2.4}$$

where the finite fourier transform $X(f,T)$ is defined by

$$X(f,T) = \int_0^T x_T(t)e^{-j2\pi ft}dt \tag{2.5}$$

and $X^*(f,T)$ is the complex conjugate of $X(f,T)$. Here $x_T(t)$ is the observed time signal $x(t)$ over the range $0 \leq t \leq T$. In practice the total acquisition time $T$ will always be finite since the limiting operation $T \to \infty$ can never be reached and hence the assumption is made that

$$\lim_{T\to\infty} X(f,T) = X(f) \tag{2.6}$$

Together with the assumption of a sufficient number of averages, for a consistent estimate, the auto spectral density function for signal $x(t)$, as given in (2.3), changes in

$$S_{xx}(f) = \frac{1}{T}X(f)X^*(f) = \frac{1}{T}|X(f)|^2 \tag{2.7}$$

The auto spectral density function for the response signal $y(t)$ can now be given by

$$S_{yy}(f) = \frac{1}{T}Y(f)Y^*(f) = \frac{1}{T}|Y(f)|^2 \tag{2.8}$$

where $Y(f)$ is the fourier transform of $y(t)$ and $Y^*(f)$ the complex conjugate of $Y(f)$. In a same way the cross spectral density function $S_{xy}(f)$ can be given by

$$S_{xy}(f) = \frac{1}{T}X^*(f)Y(f) \tag{2.9}$$

The amplitude of $S_{xy}(f)$ is the product of the amplitude of $X(f)$ and $Y(f)$ and the phase of $S_{xy}(f)$ is the difference in the phase of $X(f)$ and $Y(f)$. Comparing to $S_{xy}(f)$ the cross power spectral density function $S_{yx}(f)$ has the same amplitude but opposite phase. Conversely an auto power spectral density function has only amplitude information and no phase information is present.

### 2.1.3 Coherence Function

The coherence is an indicator for the linear dependency between two signals as function of frequency. Here it measures how much output signal $y(t)$ is a result of input signal $x(t)$. In terms of power spectral density functions the coherence function is given by

$$\gamma^2_{xy}(f) = \frac{|S_{xy}(f)|^2}{S_{xx}(f)S_{yy}(f)} \tag{2.10}$$

For all frequencies, $\gamma_{xy}^2$ satisfies

$$0 \leq \gamma_{xy}^2(f) \leq 1 \tag{2.11}$$

In the case $\gamma_{xy}^2(f) = 1$ all the measured output power is due to the input power and so a linear relationship exist and in the case $\gamma_{xy}^2(f) = 0$ the output is not related to the input. When $\gamma_{xy}^2(f)$ is between 0 and 1 it is possible that there exist a non linear relation between input and output or the system is subjected to extraneous noise. Other possibilities are leakage due to an insufficient resolution or a time delay between the two signals which is in de same order as the acquisition time. By making use of the definition that

$$S_{xy}(-f) = S_{xy}^*(f) = S_{yx}(f) \tag{2.12}$$

the coherence function can also be obtained from the ratio of estimators $H_1(f)$ and $H_2(f)$. Then the coherence function is given by

$$\gamma_{xy}^2(f) = \frac{H_1(f)}{H_2(f)} \tag{2.13}$$

With the definitions of $H_1(f)$ and $H_2(f)$ given in respectively (2.1) and (2.2) this results again in (2.10).

## 2.2 Measurement Setup

For the identification of a system SigLab can be used as the system identification device. The excitation signal $x(t)$ is generated by SigLab Virtual Function Generator (VFG) and both the excitation signal $x(t)$ and response signal $y(t)$ are measured by using the SigLab Virtual Network Analyzer (VNA). After the signals are measured also calculations can be made by VNA like power spectral density function estimates or a transfer function estimate.

### 2.2.1 Virtual Function Generator

By using VFG for generating an excitation signal $x(t)$, the Root Mean Square (RMS) value of $x(t)$, in Volts, needs to be specified. The RMS value is the square root of the Mean Square Value (MSV). For the signal $x(t)$ the MSV can be given by

$$MSV = RMS^2 = \psi_x^2 \tag{2.14}$$

and represents the time averaged power contained in signal $x(t)$ [2]. In the time domain the relation between $\psi_x^2$ and a general stationary random signal $x(t)$, over the range $0 \leq t \leq T$, is defined by

$$\psi_x^2 = \frac{1}{T}\int_0^T x_T^2(t)dt \tag{2.15}$$

With the assumption given in (2.6), the inverse of the fourier transform given in (2.5) is defined by

$$x_T(t) = \int_{-\infty}^{\infty} X(f)e^{j2\pi ft}df \tag{2.16}$$

Now by substituting $x_T(t)$ in (2.15), the time averaged power can be given in the frequency domain as

$$\psi_x^2 = \int_{-\infty}^{\infty} \frac{1}{T}|X(f)|^2 df \tag{2.17}$$

Now concentrate on the frequency band, centered at frequency $f_0$ and with a bandwidth of $\Delta f$, and assume the total power in signal $x(t)$ is constant. When input signal $x(t)$ only contains one frequency then $\psi_x^2$ equals $S_{xx}(f)$, as given in (2.7), according to

$$\lim_{\Delta f \downarrow 0} \frac{1}{\Delta f} \int_{f_0 - \frac{\Delta f}{2}}^{f_0 + \frac{\Delta f}{2}} \frac{1}{T} |X(f)|^2 df = S_{xx}(f) \tag{2.18}$$

This is plausible since all the power is present in a single frequency. When the input signal $x(t)$ is a bandwidth limited white noise the power has to be distributed over the frequencies present in the signal. The broader the frequency band, and so the larger $\Delta f$, results in a decrease of $S_{xx}(f)$ according to (2.17)

### 2.2.2 Virtual Network Analyzer

The excitation signal $x(t)$ generated by VFG and the response signal $y(t)$ can be made visible by using VNA. For measuring a signal by SigLab a sampling frequency $f_b$ and a total number of samples $N$ needs to be specified. When interested in a small frequency band with a high frequency resolution it is optional to apply zoom FFT. With a specified sampling frequency and number of samples the total acquisition time $T$ is given by

$$T = N \cdot \Delta T = \frac{N}{f_b} = \frac{1}{\Delta f} \tag{2.19}$$

where $N$ is the number of samples, $\Delta T$ is the sample period of one sample, $f_b$ is the sampling frequency with which the samples are taken and $\Delta f$ is the frequency resolution.

The spectral estimates for the auto and cross spectral density functions are computed internally to SigLab. For a more consistent estimation the number of averaging can be specified. When observing a signal with a constant ratio of $f_b$ and $N$, and so the total acquisition time is constant, the value of $S_{xx}(f)$ should be equal according to (2.7). This under the condition that the excitation signal is constant. Finally the frequency response estimation is computed by SigLab using the $H_1(f)$ estimation as given in (2.1).

# Chapter 3

# Control System

In this report the identification of a controlled fourth order system is discussed. Hereto in the first section the control system is discussed and secondly the identification of this control system.

## 3.1 Control System Description

In this report all the measurements are carried out on a fourth order system with two rotating masses which are connected with a flexibel bar. The masses are liable to friction and one of the two masses is driven by an electric motor. The electric motor is on its turn powered by an amplifier and the angular position of the two masses is detected by optical incremental encoders. Here the first mass, which is driven by the electric motor, is called the motor-mass, with an inertia $J_1$, and the second mass, with an inertia $J_2$, is called the load-mass. The two angular positions are given by respectively $\phi_1$ and $\phi_2$. The torque $T$ is assumed to be linear with the applied voltage to the amplifier. A schematic representation is given in figure 3.1. Here friction is represented by parameters $d_1$ and $d_2$ and the flexibility of the bar is represented by the parameter $k$.

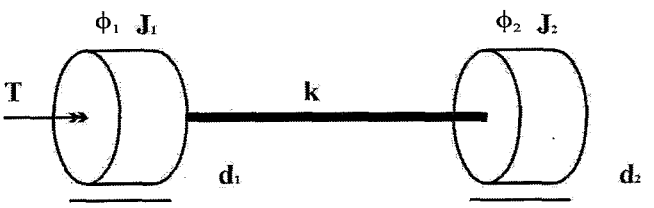


Figure 3.1: Schematic view of the fourth order system

From now on the fourth order system as well as the amplifier are part of the system. A bode diagram can be found in figure 3.2. A resonance is found at 48 Hz and an anti-resonance is found at 33 Hz. At a logarithmic frequency scale approximately a slope $-2$ can be observed for low and high frequencies. The applied voltage to the amplifier is the input of the system and the signal coming from the encoder of the motor-mass, $\phi_1$, is the output of the system. Here the input is in Volts and restricted to $\pm$ 10 Volts and the output is in radians and has an accuracy of 2000 pulses a cycle. This system is controlled with a PD-controller which is implemented on a Digital Signal Processing (DSP) controller board of dSpace, simply called dSpace board.

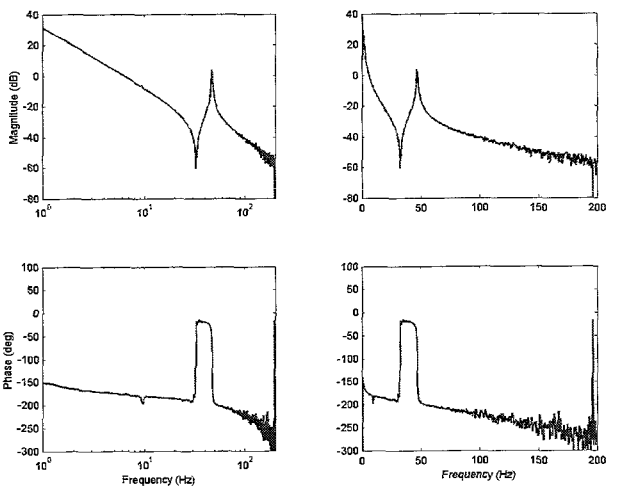


Figure 3.2: Identified Bode diagrams of the system with a logarithmic (left) and linear (right) frequency axis

## 3.2 Control System Identification

For the identification of the system SigLab is used here. As is mentioned in section 2.2 for identification purposes the VFG and VNA are used. By using VNA both the input and output signals are measured in Volts $[V]$, the spectral density function is given in $[V^2/Hz]$ and the mean square value of both the input and output signals, $\psi^2$, is given in $[V^2]$. A schematic view of the controlled system and the connection with SigLab is given in figure 3.3.

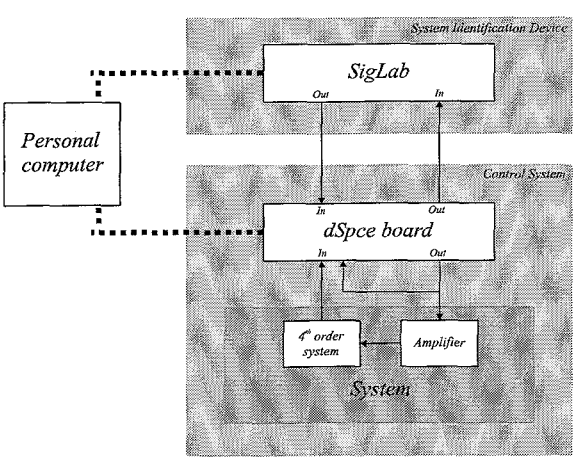


Figure 3.3: Schematic view of the controlled system connected to the identification device

# Chapter 4

# Open Loop FRF Measurement

The control system described in section 3.1 is operating in closed loop. A schematic representation of this closed system in continuous time is given in figure 4.1.

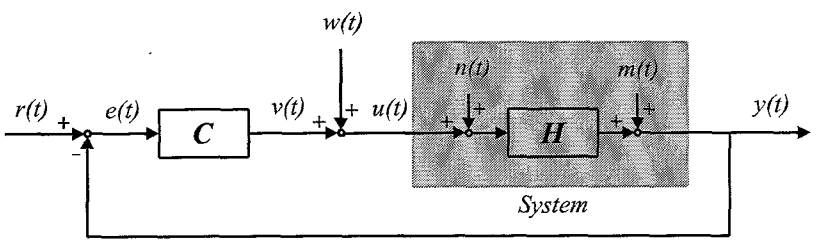


Figure 4.1: Closed loop system in continuous time

Here $C$ represents the controller and $H$ is the process representing the 4th order system and the amplifier. This process is subjected to input noise $n(t)$ and output noise $m(t)$. These noise sources and the process are assumed to be part of the system and can not be influenced.

The open loop FRF of this controlled system can be obtained by measuring the sensitivity function as well as the complementary sensitivity function [3]. In order to measure the sensitivity and complementary sensitivity function an extra input $w(t)$ is added to the control loop as is shown in figure 4.1. It is assumed that all the inputs of the closed loop system, $r(t)$, $n(t)$, $m(t)$ and $w(t)$, are uncorrelated with each other.

## 4.1 Measurement Methods

The open loop FRF of the controlled system, shown in figure 4.1 is defined here by

$$H_{ol}(f) = C(f)H(f) \tag{4.1}$$

This is obtained by observing the closed loop system without closing the feedback loop. Further the sensitivity function $S(f)$ is defined by

$$S(f) = \frac{1}{1 + C(f)H(f)} \tag{4.2}$$

Now by using the sensitivity function the open loop FRF as given in (4.1) can be calculated by

$$H_{ol}^{S}(f) = \frac{1}{S(f)} - 1 = H_{ol}(f) \tag{4.3}$$

Second the complementary sensitivity function $T(f)$ is defined by

$$T(f) = \frac{C(f)H(f)}{1 + C(f)H(f)} \tag{4.4}$$

Now by using the complementary sensitivity function the open loop FRF as given in (4.1) can be calculated by

$$H_{ol}^{T}(f) = \frac{T(f)}{1 - T(f)} = H_{ol}(f) \tag{4.5}$$

In the next sections these two methods will be used to calculate the open loop FRF out of measurements. Secondary the sensitivity as well as the Complementary sensitivity will be determined on the basis of the two system estimators $H_1$ and $H_2$. This in spite of the fact that SigLab only can use estimator $H_1$. But with these two estimators the coherence function can be determined according to (2.13).

### 4.1.1 Sensitivity Method

The sensitivity function for the closed loop system given in figure 4.1 can be determined by measuring signal $w(t)$ and $u(t)$. Estimators $H_1(f)$ and $H_2(f)$ are given by respectively

$$\begin{aligned} H_1(f) &= \frac{S_{wu}(f)}{S_{ww}(f)} \\ H_2(f) &= \frac{S_{uu}(f)}{S_{uw}(f)} \end{aligned} \tag{4.6}$$

with $S_{ww}(f)$, $S_{uu}(f)$, $S_{wu}(f)$ and $S_{uw}(f)$ as given in Appendix A this results in respectively

$$\begin{aligned} H_1(f) &= \frac{1}{1 + C(f)H(f)} \\ H_2(f) &= \frac{1}{1 + C(f)H(f)} \cdot \\ &\qquad \left( \frac{S_{ww}(f) + |C(f)|^2 S_{rr}(f) + |C(f)|^2 S_{mm}(f) + |C(f)|^2 |H(f)|^2 S_{nn}(f)}{S_{ww}(f)} \right) \end{aligned} \tag{4.7}$$

Measuring the sensitivity by using SigLab, and so using $H_1(f)$, the open loop as defined in (4.3) can be given by using $S(f) = H_1(f)$ and this results in

$$H_{ol}^{S}(f) = \frac{S_{ww}(f) - S_{wu}(f)}{S_{wu}(f)} = C(f)H(f) \tag{4.8}$$

Indeed this equals $H_{ol}$. The coherence of the sensitivity measurement is defined by

$$\gamma_{wu}^{2}(f) = \frac{S_{ww}(f)}{S_{ww}(f) + |C(f)|^2 S_{rr}(f) + |C(f)|^2 S_{mm}(f) + |C(f)|^2 |H(f)|^2 S_{nn}(f)} \tag{4.9}$$

and is exactly given by the ratio of $H_1(f)$ and $H_2(f)$.

### 4.1.2 Complementary Sensitivity Method

The complementary sensitivity function for the closed loop system given in figure 4.1 can be determined by measuring signal $w(t)$ and $v(t)$. Estimators $H_1(f)$ and $H_2(f)$ are given by respectively

$$\begin{aligned} H_1(f) &= \frac{S_{wv}(f)}{S_{ww}(f)} \\ H_2(f) &= \frac{S_{vv}(f)}{S_{vw}(f)} \end{aligned} \tag{4.10}$$

with $S_{ww}(f)$, $S_{vv}(f)$, $S_{wv}(f)$ and $S_{vw}(f)$ as given in Appendix A this results in respectively

$$\begin{aligned} H_1(f) &= \frac{-C(f)H(f)}{1+C(f)H(f)} \\ H_2(f) &= \frac{-1}{1+C(f)H(f)} \cdot \\ &\quad \left( \frac{C(f)S_{rr}(f) + C(f)S_{mm}(f) + C(f)|H(f)|^2 S_{nn}(f) + C(f)|H(f)|^2 S_{ww}(f)}{H^*(f)S_{ww}(f)} \right) \end{aligned} \tag{4.11}$$

Measuring the complementary sensitivity by using SigLab, and so using $H_1(f)$, the open loop as defined in (4.5) can be given by using $T(f) = -H_1(f)$ and this results in

$$H_{ol}^T(f) = \frac{-S_{wv}(f))}{S_{ww}(f) + S_{wv}(f)} = C(f)H(f) \tag{4.12}$$

Indeed also this equals $H_{ol}$. The coherence of the complementary sensitivity measurement is defined by

$$\gamma_{wv}^2(f) = \frac{|H(f)|^2 S_{ww}(f)}{S_{rr}(f) + S_{mm}(f) + |H(f)|^2 S_{nn}(f) + |H(f)|^2 S_{ww}(f)} \tag{4.13}$$

and is again exactly given by the ratio of $H_1(f)$ and $H_2(f)$.

## 4.2 Measurement Procedure

To eliminate the negative effects of friction a constant velocity reference trajectory is prescribed during experiments. Here the constant velocity is chosen to be 60 radians per second. Further to investigate the effect of the sampling frequency on the open loop FRF here the open loop FRF is measured at three different sampling frequencies for dSpace: $f_s = 2000$, $f_s = 1000$ Hz and $f_s = 400$ Hz. To demonstrate the effects referred in question a frequency range is selected of 0 till 2000 Hz.

For identifying the controlled system a white noise excitation signal is used. For accurate measurements, with a coherence approximating 1 also above the Nyquist frequency, small bandwidth excitation signals are chosen. This because the control system is implemented digitally, and operates on samples, and therefore aliasing effects may occur. As a consequence when adding an excitation signal, which contains frequency components above the Nyquist frequency, they will be folded around the Nyquist frequency into lower frequency components. To limit the negative effects of aliasing it is chosen to do many small bandwidth excitation measurements. The excitation frequency range is selected to be a tenth part of the dSpace sampling frequency. The corresponding number of samples is chosen such that the frequency resolution approximates 0.25 Hz.

Finally in VNA of SigLab the excitation is linked to the measurement and an output RMS of 0.4 Volts is selected. Further in VNA's channel setup all the channels are selected to have a measurement range of $-5$ till $+5$ Volts. For improving the measurement results an averaging procedure is followed. Therefore in the data processing part of VNA the number of averaging is selected to be 50 times.

# Chapter 5

# Open Loop FRF Measurement Results and Analysis

In this chapter first the open loop FRF measurement results are given in section 5.1. Secondly in section 5.2 the measurements are analyzed with a special attention to the sampling frequency dependency of all the measured open loop FRF's.

## 5.1 Measurement Results

In this section the result are given for the open loop FRF obtained by the sensitivity measurement as well as obtained by the complementary sensitivity. For both methods the open loop FRF is given for the three proposed sampling frequencies of 2000 Hz, 1000 Hz and 400 Hz.

The open loop FRF for a sampling frequency of 2000 Hz was obtained from 10 intervals of 200 Hz and 1024 samples each. The corresponding frequency resolution is 0.25 Hz. Secondly the open loop FRF for a sampling frequency of 1000 Hz was obtained from 20 intervals of 100 Hz and 512 samples each. The corresponding frequency resolution is also 0.25 Hz. A third open loop FRF is given for a sampling frequency of 400 Hz. This open loop FRF was obtained from 50 intervals of 40 Hz and 256 samples each. The corresponding frequency resolution is 0.2 Hz. These parameters are used for the sensitivity measurement as well as for the complementary sensitivity measurement.

### 5.1.1 Sensitivity Method

The open loop FRF obtained by the sensitivity method is given here. In figure 5.1 the open loop FRF is given for a sampling frequency of 2000 Hz. The given coherence measurement belongs to the corresponding sensitivity measurement. Secondly, in figure 5.2 the open loop FRF is given for a sampling frequency of 1000 Hz. A third open loop FRF is given in figure 5.3 for a sampling frequency of 400 Hz.

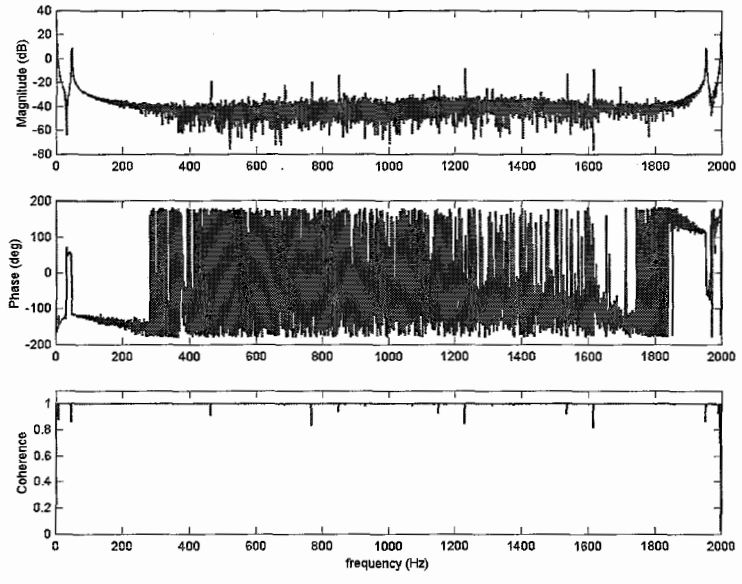


Figure 5.1: Open Loop FRF and coherence via sensitivity method for $f_s = 2000$ Hz

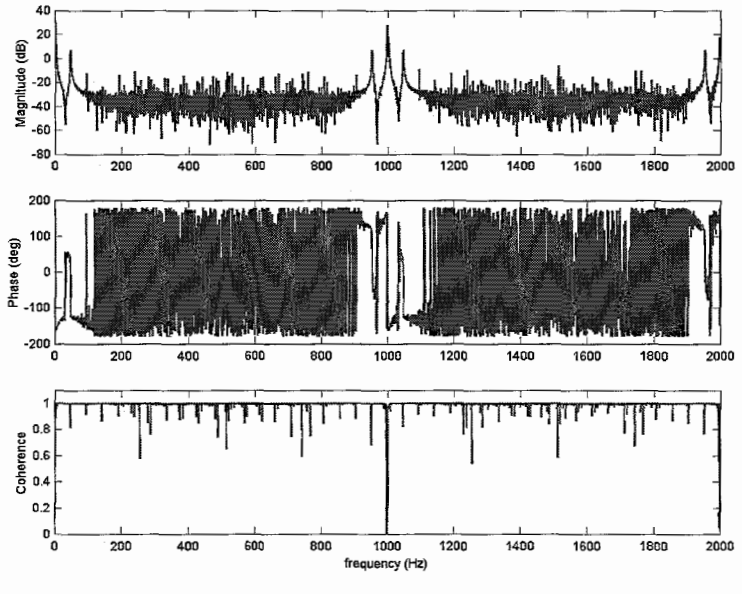


Figure 5.2: Open Loop FRF and coherence via sensitivity method for $f_s = 1000$ Hz

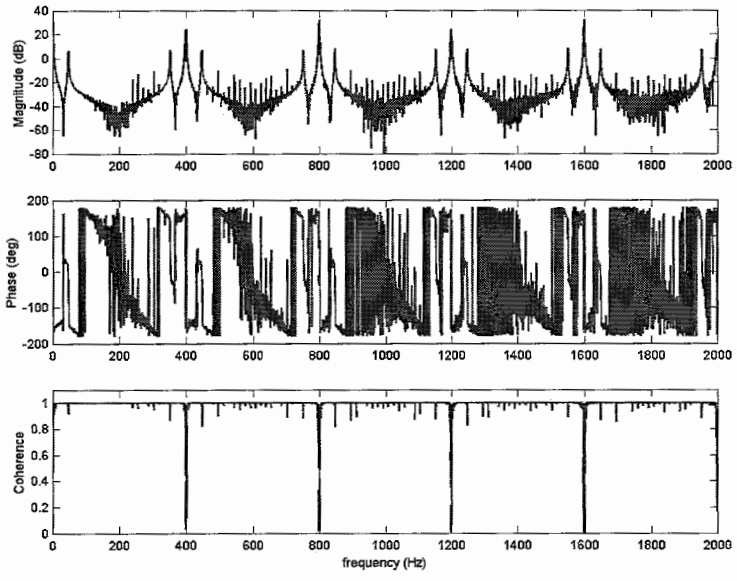


Figure 5.3: Open Loop FRF and coherence via sensitivity method for $f_s = 400$ Hz

### 5.1.2 Complementary Sensitivity Method

The open loop FRF obtained by the complementary sensitivity method is given here. In figure 5.4 the open loop FRF is given for a sampling frequency of 2000 Hz. The given coherence measurement belongs to the corresponding complementary sensitivity measurement. Secondly, in figure 5.5 the open loop FRF is given for a sampling frequency of 1000 Hz. A third open loop FRF is given in figure 5.6 for a sampling frequency of 400 Hz.

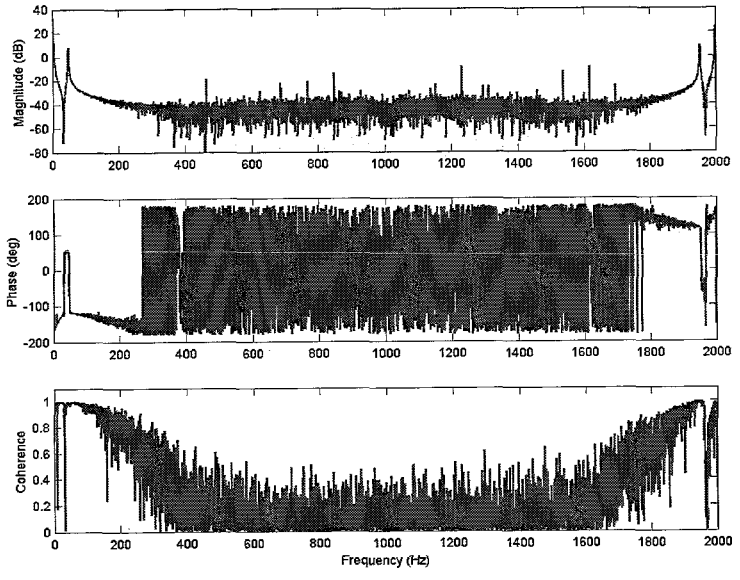


Figure 5.4: Open Loop FRF and coherence via complementary sensitivity method for $f_s = 2000$ Hz

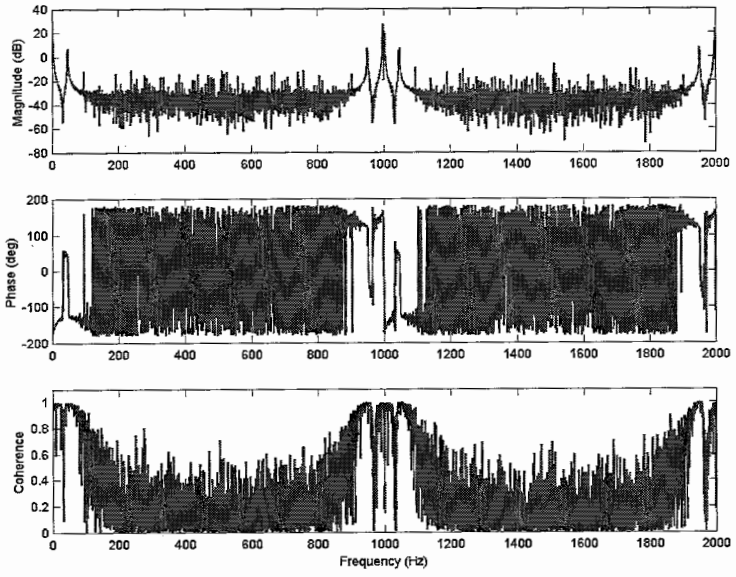


Figure 5.5: Open Loop FRF and coherence via complementary sensitivity method for $f_s = 1000$ Hz

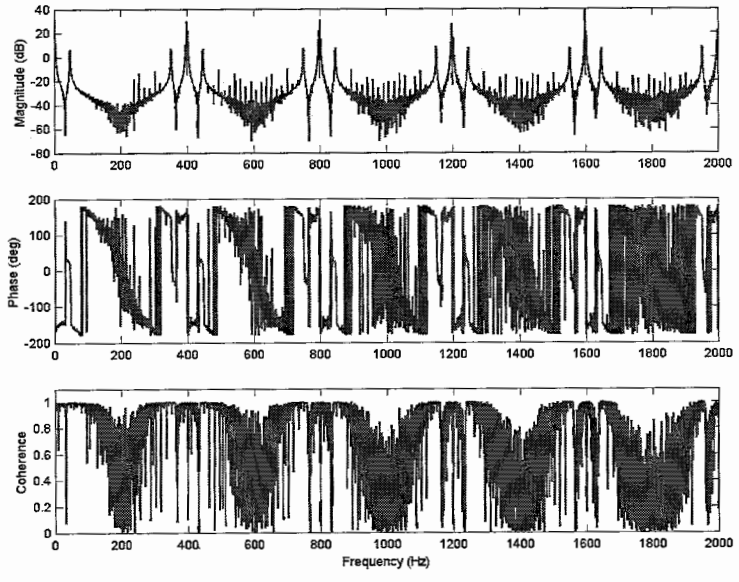


Figure 5.6: Open Loop FRF and coherence via complementary sensitivity method for $f_s = 400$ Hz

## 5.2 Measurement Analysis

Observing the measured open loop FRF's, for sensitivity and complementary sensitivity method and also for the three different sampling frequencies, they all show a resonance at 48 Hz and an anti-resonance at 33 Hz. This behavior is characteristic for the controlled fourth order system. An additional effect is that for both methods the spectrum is periodically with a period of $f_s$ Hz. Furthermore for one period of $f_s$ Hz the spectrum is folded at the Nyquist frequency (or a multiple of the Nyquist frequency). Since the measurements are done in the frequency range of 2000 Hz there is only one period of $f_s$ present for the measurement of $f_s = 2000$ Hz, for the measurement of $f_s = 1000$ Hz there are 2 periods visible and for the measurement of $f_s = 400$ Hz there are 5 periods.

When observing the phase of the open loop FRF also a certain periodicity with $f_s$ can be found. A difference with the periodicity in magnitude is that at the Nyquist frequency the phase spectrum is not only folded around the Nyquist frequency but also folded around the 0 degree axis. In other words the phase spectrum shows symmetry in two directions at multiples of the point $f_s$ Hz and the 0 degree axis. The behavior of phase and magnitude is due to aliasing effects and results from the fact that the system operates on samples.

Further observing the magnitude of both measurement methods, for high gains the variance on the signal is small in stead of the variance on the signal for low gains, which is large. This is caused by the fact that at the low gains an (small) output noise is dominating the signal and that at the high gains a (small) noise contamination does not affect the magnitude. This effect at low gains is mainly due to the resolution of the incremental encoder and will be discussed in more detail in section 6.1. Consequently, the variance in magnitude can also be observed in the phase. Here a strong fluctuating phase can be seen.

Concerning the magnitude and phase, it can be concluded that the differences in the open loop FRF measurements via sensitivity and complementary sensitivity are negligible. There is only a difference in the indicated quality of the measurements. The given coherence measurements belong to the sensitivity measurements and the complementary sensitivity measurements. These measurements are shown in Appendix C. Observing (4.9) and in the case there is extraneous noise, the coherence of the sensitivity measurement should approach 1 at a low process gain ($|H(f)| << 1$). On contrary, for a high process gain the coherence should diminished. For the coherence of the process sensitivity, given in (4.13) and again in the case there is extraneous noise, a coherence approaching 1 should be obtained at high process gains and a low coherence should be obtained at low process gains. Comparing the theory to the measurements there is a strong similarity and therefore, in spite of the differences between the two methods, the coherence behavior is what is expected.

Another notable aspect in the coherence measurements are the local decreases, which look to have a certain periodicity. In fact, these local decreases only appear in the frequency range from 0 Hz till the Nyquist frequency. Other local decreases are only aliased similarities. Although there is no explanation for this phenomena found, it could be jogging related. A simple test while changing the jogging velocity should reveal the jogging dependency.

In chapter 4 the calculated open loop FRF was based on a continuous time closed loop system. Since aliasing effects occur, it means that the system operates on samples. So in fact we are dealing with a sampled data system. Now to explain the measurement results the analog as well as the digital parts, and the necessary interface to connect the analog and digital world, has to be taken into account. Therefore in next chapter a mixed analog and digital closed loop system is considered.

# Chapter 6

# Implemented Closed Loop System

In chapter 4 the closed loop system was considered in continuous time, but as was mentioned in section 3.1 the controller was implemented digitally. Such a digital control system or sampled data system includes several unique components not found in a continuous control system. A schematic view of the implemented closed loop system, with all its components, is given in figure 6.1.

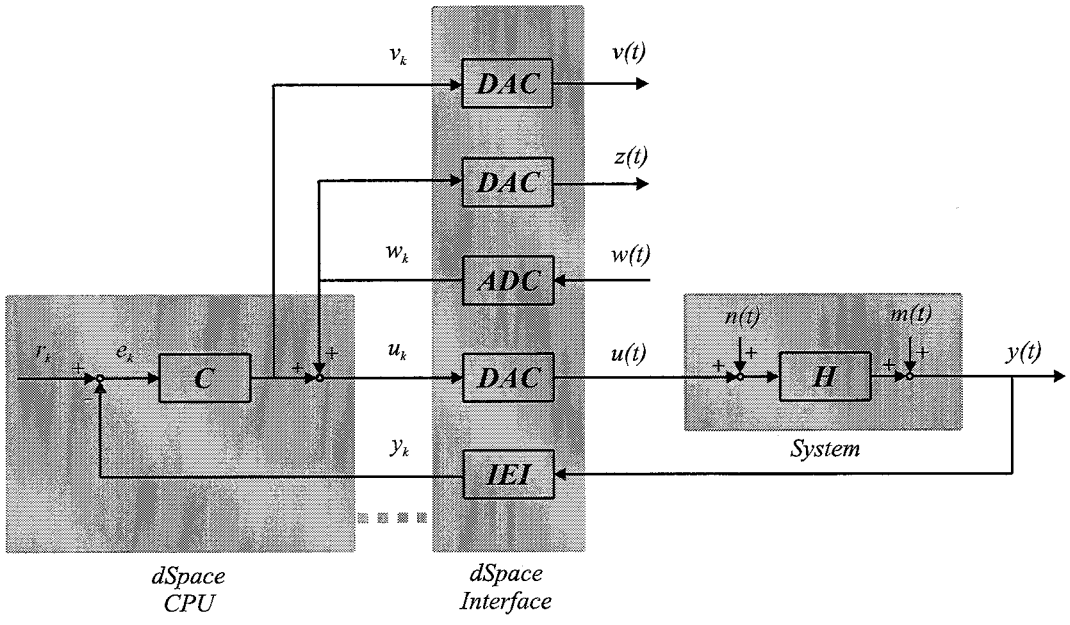


Figure 6.1: Implemented closed loop system

The configuration of this closed loop system is for measuring the sensitivity function and the complementary sensitivity function. This closed loop system can be divide in three parts. The first part is the system. This system is an analog system, which contains a process $H$ and noise sources $n(t)$ and $m(t)$, and is equivalent to the system used in chapter 4. The second part is the dSpace Central Processing Unit ($CPU$), which performs all the necessary calculations for the control action. This is represented by $C$. The last part is the dSpace interface [4]. This interface connects the analog outside world with the digital controller. In this case the used units of the interface are the Analog to Digital Converter

($ADC$) unit, the Digital to Analog Converter ($DAC$) unit and the Incremental Encoder Interface ($IEI$) unit. These units are discussed in more detail in the next section.

## 6.1 dSpace Interface

### 6.1.1 Analog to Digital Conversion

The ADC unit of the dSpace interface is a device that converts the voltage of the input signal to a binary number usable by a computer. In other words the continuous input signal is digitized. What happens during the digitalization is that first the signal is repeatedly observed at regular instants of $\Delta T$ seconds. Here $\Delta T$ represents the sample period between two successive samples. The relation with the sampling frequency $f_s$ is given by

$$f_s = \frac{1}{\Delta T} \tag{6.1}$$

where $\Delta T$ is given in seconds and $f_s$ is given in Hertz. Now the continuous signal becomes a discrete signal. Another aspect performed by the ADC unit is the quantization of the signal. This makes the signal also not continuous in magnitude and amplitude. Now the discrete signal is represented by a sequence of binary numbers. Such a binary number consists of bits. In case of the dSpace interface the number of bits of input channels 1 and 2 is given by 16 and input channels 3 and 4 have 12 bits. In the case of 12 bits one can represent $2^{12} = 4096$ numbers, and therefore an ADC unit with 12-bits is said to have a resolution of $1/4096$. The time it takes to convert the signal for input channels 1 and 2 is about $4\mu s$ and the conversion time of channels 3 and 4 is $1.25\mu s$ each.

In figure 6.1 the voltage of the input signal to the ADC unit is represented by $w(t)$. Given a sampling period of $\Delta T$ seconds, the sequence of binary numbers is given by $w(kT)$ or with a little abuse of notation by $w_k$, where $k$ is an integer.

### 6.1.2 Digital to Analog Conversion

The DAC unit is an other part of interfacing the digital controller with the outside world. This unit converts binary numbers into analog voltages. For the dSpace interface all the output channels provides 12 bits. First of all the output signal is only known at regular instants of $\Delta T$ seconds. Therefore a second circuitry, a hold circuit, is used in the conversion to make the signal a continuous time signal. In figure 6.1 the voltage of the output signals of the DAC unit are represented by $u(t)$, $v(t)$ and $z(t)$. The inputs of the DAC unit are binary numbers and represented by $u_k$, $v_k$ and $w_k$. Finally in contrary to the ADC unit the DAC unit is not subjected to conversion time.

### 6.1.3 Incremental Encoder Interface

Since at the output of the system an incremental encoder is used, the IEI interface of the dSpace board is used. This interface contains a 24 bits absolute position counter to read the position of the incremental encoder. The incremental encoder has a codewheel with 500 window and bar pairs. For each pair there are given 4 counts. Now 500 window pairs corresponds to 2000 encoder lines. So the position in radians $\phi$ is given by.

$$\phi = 2^{23} \cdot \frac{2 \cdot \pi}{encoderlines} \tag{6.2}$$

In fact the incremental encoder together with the IEI unit is nothing else than digitizing the angular position of one of the two masses. The corresponding resolution is in order of magnitude given by

$$\frac{2 \cdot \pi}{encoderlines \cdot \left(u_{max}(t) - u_{min}(t)\right)} \tag{6.3}$$

In the case of 2000 encoder lines and a maximum system input between $-10$ Volt and $+10$ Volt, the resolution of the magnitude is given by approximately $-76$ dB. So a magnitude of less than $-76$ dB has no significance at all.

## 6.2 Open Loop FRF Measurement

To have a try to explain the effects of the dSpace interface on the open loop FRF here again the open loop FRF of the system in figure 6.1 is calculated by using the sensitivity function and the complementary sensitivity function. Therefore in this figure $C$ and $H$ are used in the same way as they were used in figure 4.1.

### 6.2.1 Sensitivity Method

The sensitivity function for the implemented closed loop system given in figure 6.1 can be determined by measuring signal $z(t)$ and $u(t)$. Estimators $H_1(f)$ and $H_2(f)$ are given by respectively

$$\begin{aligned} H_1(f) &= \frac{S_{zu}(f)}{S_{zz}(f)} \\ H_2(f) &= \frac{S_{uu}(f)}{S_{uz}(f)} \end{aligned} \tag{6.4}$$

with $S_{zz}(f)$, $S_{uu}(f)$, $S_{zu}(f)$ and $S_{uz}(f)$ as given in Appendix B this results in respectively

$$\begin{aligned} H_1(f) &= \frac{1}{1 + DAC(f)C(f)IEI(f)H(f)} \\ H_2(f) &= \frac{1}{1 + DAC(f)C(f)IEI(f)H(f)} \Big( \frac{S_{zz}(f) + |ADC(f)|^2|DAC(f)|^2|C(f)|^2 S_{rr}(f)}{S_{zz}(f)} \\ &\quad + \frac{|DAC(f)|^2|C(f)|^2|IEI(f)|^2 S_{mm}(f) + |DAC(f)|^2|C(f)|^2|IEI(f)|^2|H(f)|^2 S_{nn}(f)}{S_{zz}(f)} \Big) \end{aligned} \tag{6.5}$$

Measuring the sensitivity by using SigLab, and so using $H_1(f)$, the open loop as defined in (4.3) can be given by using $S(f) = H_1(f)$ by

$$H_{ol}^{S}(f) = \frac{S_{zz}(f) - S_{zu}(f)}{S_{zu}(f)} = DAC(f)C(f)IEI(f)H(f) \tag{6.6}$$

The coherence of the sensitivity measurement is defined by

$$\gamma_{zu}^2(f) = \frac{S_{zz}(f)}{S_{zz}(f) + |ADC(f)|^2|DAC(f)|^2|C(f)|^2 S_{rr}(f) + |DAC(f)|^2|C(f)|^2|IEI(f)|^2 S_{mm}(f) + |DAC(f)|^2|C(f)|^2|IEI(f)|^2|H(f)|^2 S_{nn}(f)} \tag{6.7}$$

and is exactly given by the ratio of $H_1(f)$ and $H_2(f)$.

### 6.2.2 Complementary Sensitivity Method

The complementary sensitivity function for the implemented closed loop system given in figure 6.1 can be determined by measuring signal $z(t)$ and $v(t)$. Estimators $H_1(f)$ and $H_2(f)$ are given by respectively

$$\begin{aligned} H_1(f) &= \frac{S_{zv}(f)}{S_{zz}(f)} \\ H_2(f) &= \frac{S_{vv}(f)}{S_{vz}(f)} \end{aligned} \tag{6.8}$$

with $S_{zz}(f)$, $S_{vv}(f)$, $S_{zv}(f)$ and $S_{vz}(f)$ as given in Appendix B this results in respectively

$$\begin{aligned} H_1(f) &= \frac{-DAC(f)C(f)IEI(f)H(f)}{1+DAC(f)C(f)IEI(f)H(f)} \\ H_2(f) &= \frac{|DAC(f)|^2}{1+DAC(f)C(f)IEI(f)H(f)} \Big( \frac{|ADC(f)|^2|C(f)|^2 S_{rr}(f) + |C(f)|^2|IEI(f)|^2 S_{mm}(f)}{S_{zz}(f)} \\ &\qquad + \frac{|C(f)|^2|IEI(f)|^2|H(f)|^2 S_{nn}(f) + |C(f)|^2|IEI(f)|^2|H(f)|^2 S_{zz}(f)}{S_{zz}(f)} \Big) \end{aligned} \tag{6.9}$$

Measuring the complementary sensitivity by using SigLab, and so using $H_1(f)$, the open loop as defined in (4.5) can be given by using $T(f) = -H_1(f)$ and this results in

$$H_{ol}^T(f) = \frac{-S_{zv}(f))}{S_{zz}(f) + S_{zv}(f)} = DAC(f)C(f)IEI(f)H(f) \tag{6.10}$$

The coherence of the complementary sensitivity measurement is defined by

$$\gamma_{zv}^2(f) = \frac{-C(f)IEI(f)H(f)}{DAC(f)} \cdot \Big( \frac{S_{zz}(f)}{|ADC(f)|^2|C(f)|^2 S_{rr}(f) + |C(f)|^2|IEI(f)|^2 S_{mm}(f) + |C(f)|^2|IEI(f)|^2|H(f)|^2 S_{nn}(f) + |C(f)|^2|IEI(f)|^2|H(f)|^2 S_{zz}(f)} \Big) \tag{6.11}$$

and is again exactly given by the ratio of $H_1(f)$ and $H_2(f)$.

### 6.2.3 Comparison Closed Loop Systems

In section 4.1 the obtained result of the open loop FRF calculation is, for the sensitivity measurement as well as the complementary sensitivity measurement, given by

$$H_{ol}(f) = C(f)H(f) \tag{6.12}$$

The results of the open loop FRF calculations obtained in this section for the digital control system is, also for the sensitivity measurement as well as for the complementary sensitivity measurement, given by

$$H_{ol}(f) = DAC(f)C(f)IEI(f)H(f) \tag{6.13}$$

Now comparing the open loop FRF of (6.12) to the open loop FRF of (6.13) shows a difference of two components. These components are the DAC unit and the IEI unit. To explain the behavior of the open loop measurement results of chapter 5 in the next chapter the components of (6.13) are discussed in more detail separately.

# Chapter 7

# Closed Loop Components

In this chapter the dependence of the DAC unit, the IEI unit and also the controller $C$ and the process $H$ on different sampling frequencies is discussed.

## 7.1 DAC unit

As mentioned in section 6.1 the DAC unit is used to convert a digital signal into an analog signal. For doing only measurements on this DAC unit a digital signal needs to specified inside the computer and a measurement has to be taken at the output. A problem is that in this way it is difficult to specify the quality of the measurement and no clear understanding is gained of the time delay and the corresponding phase lag. Therefore first the combined situation of the ADC unit and the DAC unit is considered. A schematic representation of this ADC-DAC system, with input and output error sources, is given in figure 7.1. Now the input signal as well as the output signal can be measured by using SigLab.

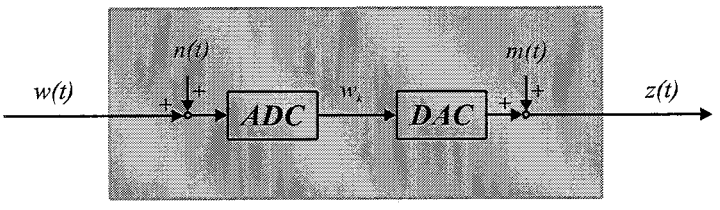


Figure 7.1: The ADC-DAC system

This ADC-DAC system is excited, at $w(t)$, with a single sinus of 100 Hz for a sampling frequency of 400 Hz, 1000 Hz and 2000 Hz. The response signal $z(t)$ for these sampling frequencies is given in figure 7.2. Now it can be seen that each value $z(t)$ is held constant, after a small delay of the ADC unit and transient phenomenon, during a period of $\Delta T$ seconds till the next value is available. For $f_s = 400$ Hz here $\Delta T = 0.0025$ seconds. As expected this is according to (6.1) and this relation applies for every sampling frequency. The behavior of figure 7.2 appears to be the Zero Order Hold (ZOH) effect. Therefore in the next section the theory of the ZOH is discussed.

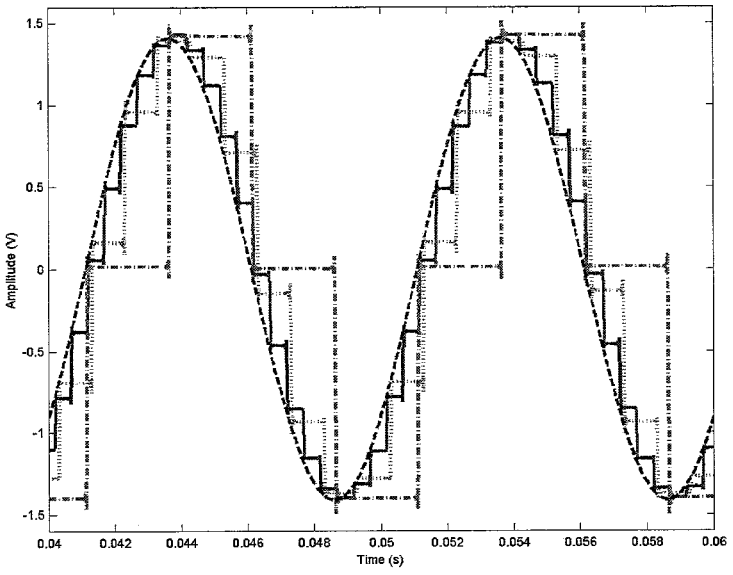


Figure 7.2: Output ADC-DAC system $z(t)$ for $f_s = 2000$ Hz (solid), $f_s = 1000$ Hz (dotted) and $f_s = 400$ Hz (dash-dotted)

### 7.1.1 Theory Zero Order Hold

In the Laplace domain the ZOH can be characterized by a transfer function

$$H_{ZOH}(s) = \frac{1 - e^{-s\Delta T}}{s} \tag{7.1}$$

where $\Delta T$ again represents the sample period [5]. This transfer function describes the relation between the discrete signal at the input and the continuous signal at the output. A bode diagram of this transfer function is given in figure 7.3. The FRF of this transfer function for the ZOH is given by (7.1) for $s = j2\pi f$. This FRF can be approximated by

$$H_{ZOH}(f) = \Delta T \cdot \frac{sin(\pi f \Delta T)}{\pi f \Delta T} \cdot e^{-j\pi f \Delta T} \tag{7.2}$$

The magnitude of this FRF is now given by

$$\left|H_{ZOH}(f)\right| = \Delta T \left|\frac{sin(\pi f \Delta T)}{\pi f \Delta T}\right| \tag{7.3}$$

and with

$$\lim_{f \downarrow 0} \left|H_{ZOH}(f)\right| = \Delta T \tag{7.4}$$

For the three different sample frequencies of 400 Hz, 1000 Hz and 2000 Hz used here, the sample periods, in decibels, are given by respectively $-52$, $-60$ and $-66$. The phase lag as function of frequency of (7.2), in degrees, can be approximated by

$$\Delta\varphi_{ZOH}(f) = -180 \cdot f \cdot \Delta T \tag{7.5}$$

This phase lag corresponds to a time delay, in seconds, is given by

$$\Delta t = \frac{\Delta\varphi}{360 \cdot f_{\Delta\varphi}} \tag{7.6}$$

Here $\Delta\varphi$ is the phase lag at the corresponding frequency $f_{\Delta\varphi}$. With the phase lag of the ZOH given in (7.5) and relation (7.6) with $\Delta\varphi = \Delta\varphi_{ZOH}$ this results in a time delay of

$$\Delta t = \frac{\Delta T}{2} \tag{7.7}$$

This is half the sample period and can also be found in the figure 7.2.

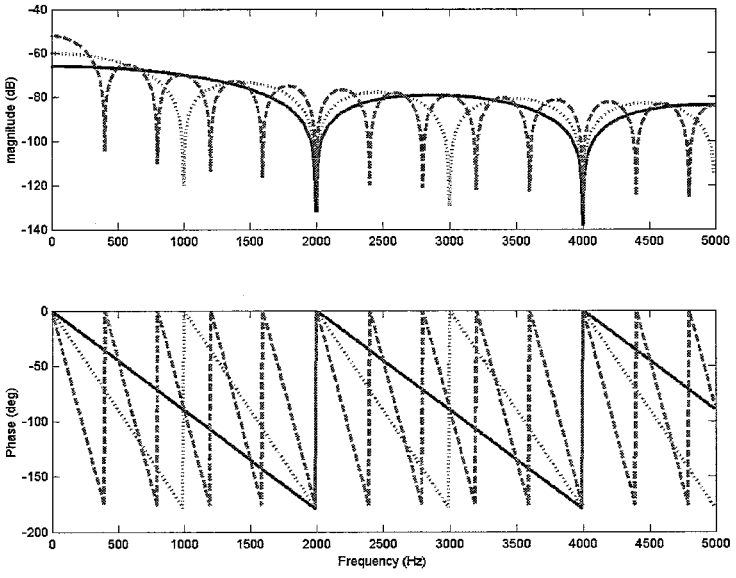


Figure 7.3: Magnitude and phase of the ZOH in theory for $f_s = 400$ Hz (dashed), $f_s = 1000$ Hz (dotted) and $f_s = 2000$ Hz (solid)

### 7.1.2 ADC-DAC system FRF measurement

When indeed a ZOH is included in the ADC-DAC system the behavior given in the bode diagram of figure 7.3 also should appear when estimating a transfer function of the ADC-DAC system. By using the $H_1$ estimator the FRF of the ADC-DAC system can be obtained by

$$H_{ADC-DAC}(f) = \frac{S_{wz}(f)}{S_{ww}(f)} = ADC(f)DAC(f) \tag{7.8}$$

The corresponding coherence function is given by

$$\gamma^2_{wz} = \frac{|ADC(f)DAC(f)|^2 S_{ww}}{S_{mm} + |ADC(f)DAC(f)|^2 S_{ww} + |ADC(f)DAC(f)|^2 S_{nn}} \tag{7.9}$$

Now for measuring the FRF the same procedure is followed as is given in section 4.2 with measurement intervals chosen as given in section 5.1. The resulting FRF's are given in figures 7.4, 7.5 and 7.6 for respectively $f_s = 2000$ Hz, $f_s = 1000$ Hz and $f_s = 400$ Hz. Furthermore to investigate the system properties at high frequencies, in figure 7.7 the measurement results are given for the frequency range from 18 kHz till 19 kHz.

Secondly the measurements are compared to the ZOH theory given in section 7.1.1. Therefore first the theoretical FRF, given by (7.2), is divided by a factor $\Delta T$. This new obtained FRF is compared to the measured FRF of the ADC-DAC system. The differences in magnitude and also the differences in phase of these two FRF's are given in figures 7.8, 7.9, 7.10 and 7.11 for respectively $f_s = 2000$ Hz, $f_s = 1000$ Hz and $f_s = 400$ Hz.

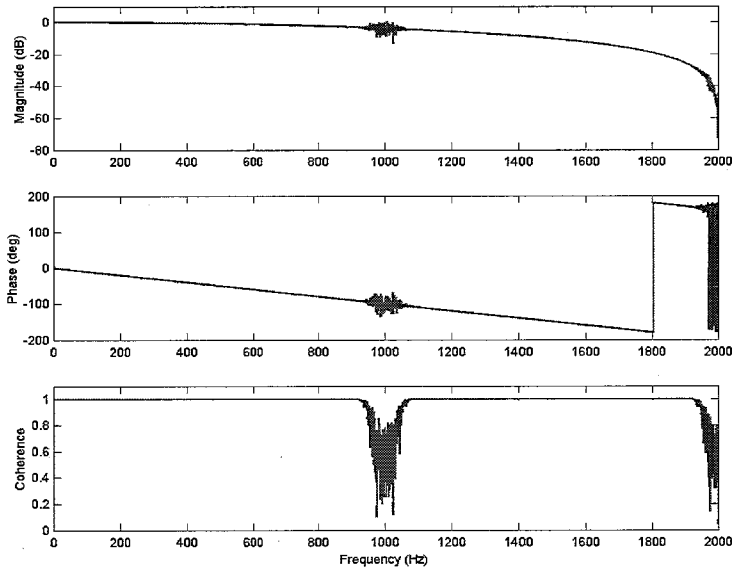


Figure 7.4: FRF and coherence of the ADC-DAC system for $f_s = 2000$ Hz

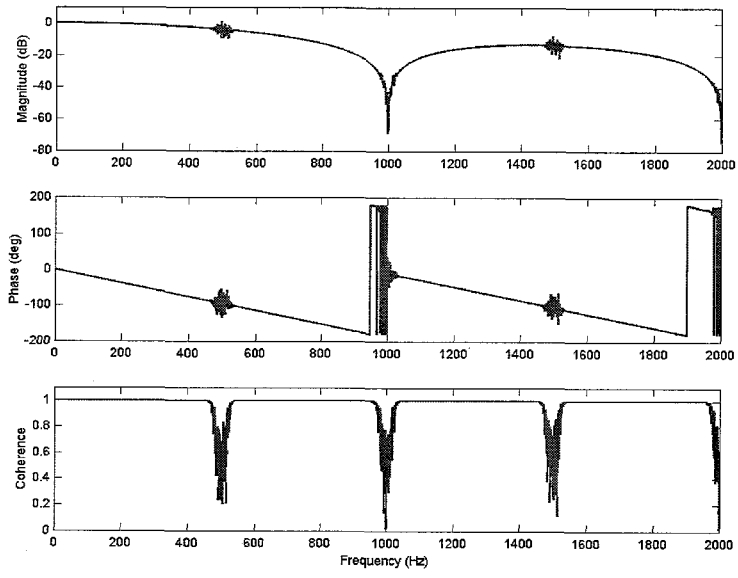


Figure 7.5: FRF and coherence of the ADC-DAC system for $f_s = 1000$ Hz

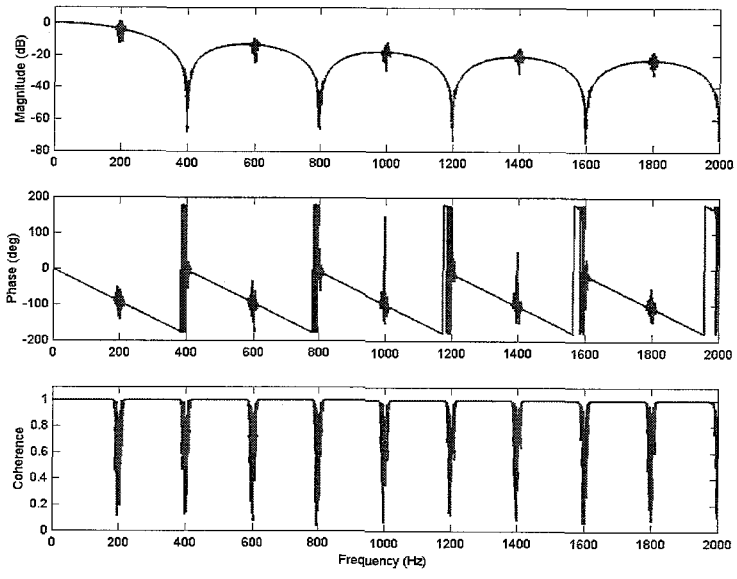


Figure 7.6: FRF and coherence of the ADC-DAC system for $f_s = 400$ Hz

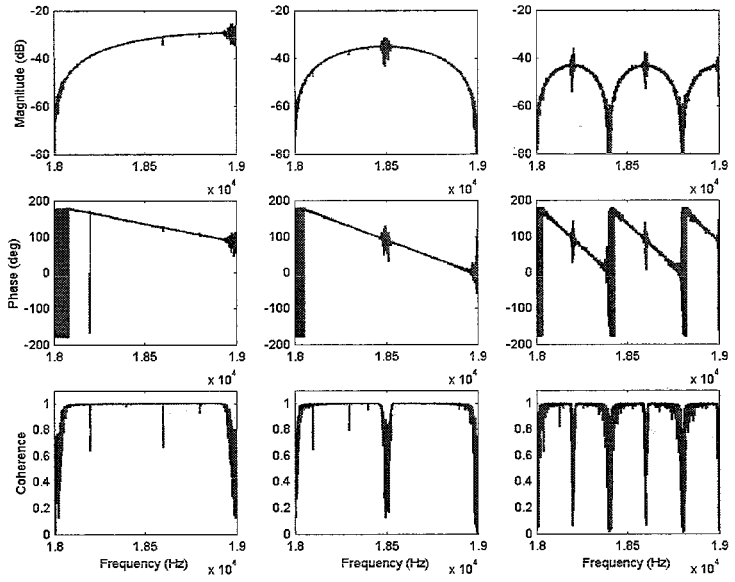


Figure 7.7: FRF and coherence of the ADC-DAC system for $f_s = 2000$ Hz (left), $f_s = 1000$ Hz (center) and $f_s = 400$ Hz (right) between 18 kHz and 19 kHz.

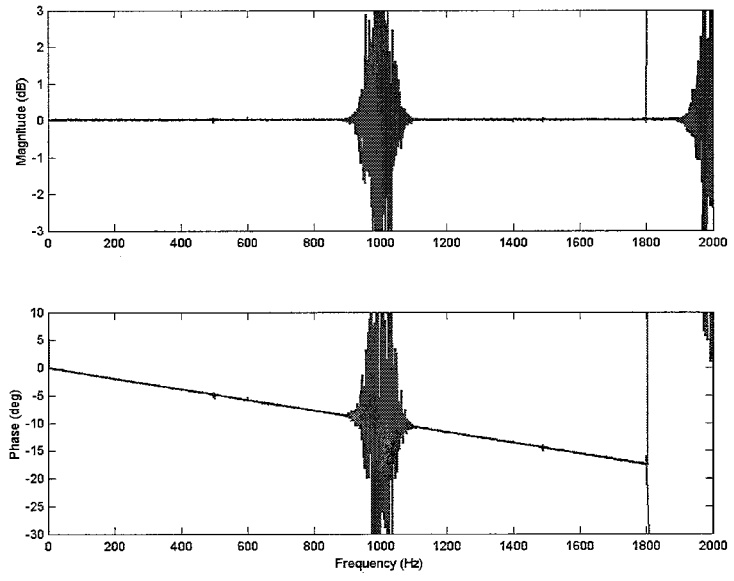


Figure 7.8: The difference with theory for $f_s = 2000$ Hz

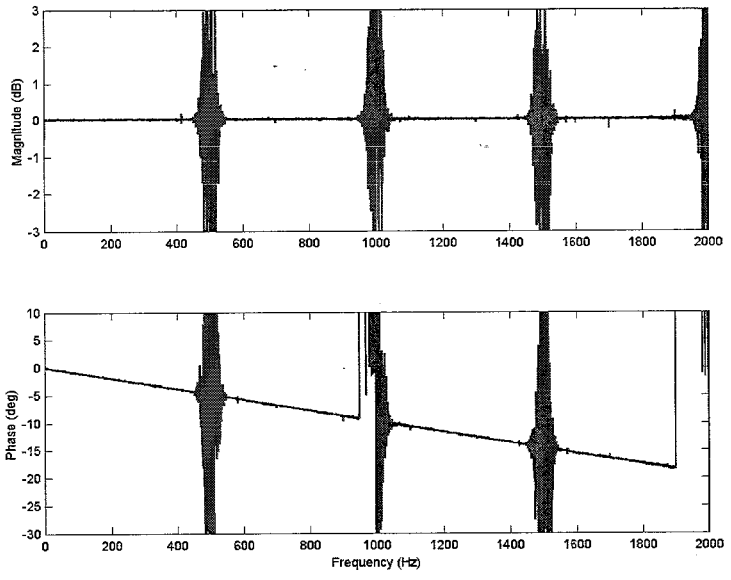


Figure 7.9: The difference with theory for $f_s = 1000$ Hz

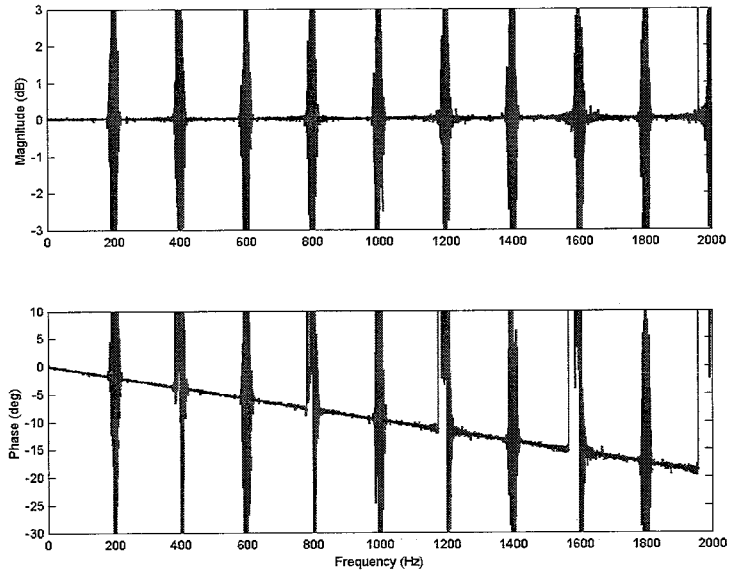


Figure 7.10: The difference with theory for $f_s = 400$ Hz

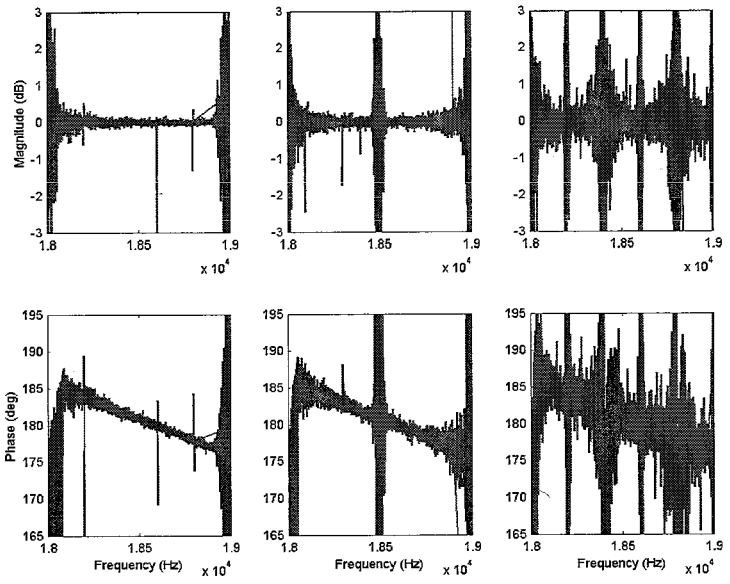


Figure 7.11: The difference with theory for $f_s = 2000$ Hz (left), $f_s = 1000$ Hz (center) and $f_s = 400$ Hz (right) between 18 kHz and 19 kHz.

Now observing figures 7.8, 7.9, 7.10 and 7.11. The difference in magnitude is negligible except at multiples of the sampling frequency and at multiples of the Nyquist frequency. At these frequencies a large variance on the magnitude can be observed and consequently this results in a fluctuating phase. Furthermore a corresponding local decrease in coherence measurement can be observed in figures 7.4, 7.5, 7.6 and 7.7. The low coherence measurement at multiples of the sampling frequency corresponds to the fact that noise sources will become dominant at low ADC-DAC system magnitudes and can also be obtained from (7.9).

Secondly, at the Nyquist frequency, the low coherence measurement is a consequence of the effect of aliasing. In theory, when using a white noise excitation signal, a frequency range from 0 Hz till maximum half the sampling frequency could be chosen without aliasing effects. But, in practice, an additional effect of bandwidth limited signals is the existence of rippled side lobes. The side lobes exceed the selected bandwidth and its amplitudes fade out with increasing frequency, and so does the spectral energy. This is demonstrated in figure 7.12, by means of auto spectral density functions, for three different bandwidth limited signals namely from 0 Hz till respectively half the Nyquist frequency, the Nyquist frequency itself and twice the Nyquist frequency. From the ADC-DAC system output measurements and the coherence measurements, as given in figure 7.12, it follows that aliasing effects occur. This way the bandwidth excitation signal from 0 till 1000 Hz only has a linear input-output relation till 400 Hz and so indicates the coherence. Indeed it is difficult to measure how much of the output signal is a result of the input signal since the energy present in frequency components above the Nyquist frequency disturb the energy present in the frequency components below the Nyquist frequency.

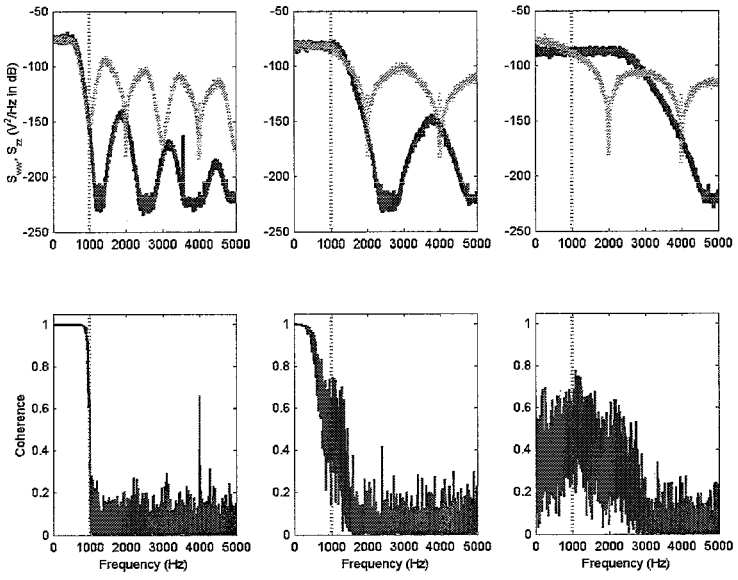


Figure 7.12: Auto spectral density function of input w(t) (solid) and output z(t) (dotted) of the ADC-DAC system (top figures) and corresponding coherence measurement between w(t) and z(t) (bottom figures). The results are given for different excitations signals with a bandwidth of 500 Hz (left), 1000 Hz (center) and 2000 Hz (right). The corresponding Nyquist frequency is at 1000 Hz (dashed).

Aliasing effects, as demonstrates in figure 7.12, are also present in the measurements of figures 7.4 till 7.7. Although here only small bandwidth excitations are selected the phenomena of a large variance on the magnitude and the corresponding diminishing coherence is still there around the Nyquist frequency. By doing even smaller bandwidth excitations, only a decrease in the covered frequency range, where aliasing effects occur, will be obtained.

Further a general tendency of an additional phase lag can be seen in figures 7.8, 7.9, 7.10 and 7.11. This phase delay is independent of the sampling frequency and is linear with the frequency. The amount of phase lag is given by 10 degrees for every 1000 Hz. According to (7.6) the corresponding time delay is 27.8 $\mu$s. This time delay could be consist of a delay due to the conversion time of signals in the ADC unit and DAC unit. As mentioned in section 6.1 the DAC unit is not subjected to conversion time, whereas the ADC unit has a conversion time of maximum 4 $\mu$s. This corresponds to a phase lag of approximately 1.5 degrees at 1000 Hz. Other reasons could be found in the non-symmetry of dSpace channels and SigLab channels. In [6] a maximum phase lag of 2 degrees at 1000 Hz, which gives a corresponding time delay of 5.6 $\mu$s, was obtained out of measurements. So the reasons mentioned only have a small contribution to the phase lag measured here but are inadequate to describe totally the measured phase behavior of the ADC-DAC system. Furthermore, since even at high frequencies there is no decrease in magnitude, the existence of a Bessel filter in de closed loop system is unlikely.

Finally since it is expected that the ZOH is part of the DAC unit, the factor $\Delta T$ in magnitude still has to be explained. Possibly this factor is part of the ADC unit and therefore this will be discussed next.

### 7.1.3 ADC unit

In this section the contribution of the ADC unit on the ADC-DAC system FRF is investigated. Observing figure 7.1, the ADC unit connects the analog input signal $w(t)$ to the discrete signal $w_k$. By analogy with (2.17), the time averaged power contained in a stationary random continuous time signal $w(t)$, in the range $0 \leq t \leq T$, can be given by

$$\psi_w^2 = \frac{1}{T}\int_{-\infty}^{\infty} w^2(t)dt \tag{7.10}$$

In the frequency domain the time averaged power can be represented by

$$\psi_w^2 = \int_{-\infty}^{\infty} S_{ww}(f)df \tag{7.11}$$

where the auto power spectral density, $S_{ww}(f)$, gives the power per Hertz and is defined by

$$S_{ww}(f) = \frac{1}{T}|W(f)|^2 \tag{7.12}$$

Here $W(f)$ is the fourier transform of $w(t)$. Similarly an averaged power contained in a discrete time signal can be given [7]. The averaged power for discrete time signal $w_k$ can be represented by

$$\psi_{w_k}^2 = \frac{\Delta T}{N}\sum_{k=0}^{N-1} w_k^2 \tag{7.13}$$

Here $N$ is the number of samples and the factor $\Delta T$ originates from the fact that the power in the discrete signal can be approximated by considering

$$w(t) = \Delta T w_k \tag{7.14}$$

By using the inverse discrete fourier transform defined by

$$w_k = \sum_{n=0}^{N-1} W_n e^{j2\pi\frac{kn}{N}} \tag{7.15}$$

it follows for the averaged power that

$$\psi_{w_k}^2 = \Delta T \sum_{k=0}^{N-1} S_{w_k w_k}(n) \tag{7.16}$$

where $S_{w_k w_k}(n)$ is the power per sample of the discrete time signal $w_k$, and is defined by

$$S_{w_k w_k}(n) = \frac{1}{N}|W_n|^2 \tag{7.17}$$

and where $W_n$ is the discrete fourier transform of $w_k$. Now $S_{ww}(f)$ becomes proportional to $S_{w_k w_k}(n)$ by the sample period $\Delta T$ according to

$$S_{ww}(f) = \Delta T S_{w_k w_k}(n) \tag{7.18}$$

So whereas premultiplying with $\Delta T$ in relation (7.2) relates the digital world to the analog world, so does $\Delta T$ in relation (7.18) in the opposite direction. It should be noted that in the case $w(t)$ is given in Volt, $S_{ww}(f)$ has the unit of square Volt per Hertz, and $S_{w_k w_k}(n)$ has the unit of square volt.

### 7.1.4 Conclusion DAC and ADC unit

In this section the behavior of the ADC-DAC system, as given in figure 7.1, is investigated. Here the final relations are given. In general for the ADC unit the relation between the analog and digital world is given in the laplace domain by

$$ADC(s) = \frac{1}{\Delta T} \tag{7.19}$$

This relation only affects the magnitude. For the DAC unit the transfer function is, in general, given by the transfer function of the ZOH

$$DAC(s) = \frac{1 - e^{-s\Delta T}}{s} \tag{7.20}$$

This transfer function describes the relation between a discrete time signal and a continuous time signal. In stead of the ADC unit this relation affects both the magnitude and phase. In both relations the sampling frequency dependency is clear since $\Delta T$ relates $f_s$ according to (6.1).

The relations given in (7.19) and (7.20) are not sufficient to describe the measured ADC-DAC system behavior. Since the DAC unit shows the ZOH system behavior, with its typically low system gains at multiples of the sampling frequencies, the local decrease in coherence measurements at multiples of the sampling frequencies is assumed to be a consequence of the DAC unit. This since noise contamination dominates at low system gains. Further, since the ADC unit is involved in the sampling of signals, the local decrease in coherence measurements at multiples of the Nyquist frequency is completely subscribed to the ADC unit. This also becomes likely when comparing (6.13) to the measurements in figures 5.1, 5.2 and 5.3. Since in (6.13) the ADC unit is not present and no local decrease in coherence measurements is obtained, in the figures mentioned, it is unlikely that the dip in coherence near the Nyquist frequency should subscribed to the DAC unit.

Finally an additional phase lag is measured as is shown in figures 7.8 till 7.11. Although there is time delay due to the conversion time of signals in the ADC unit and DAC unit and that there could be a non-symmetry in dSpace channels and SigLab channels, these reasons do not cover the obtained measured system behavior.

## 7.2 Controller $C$

Another component of the open loop FRF given by (6.13) is the FRF of the controller $C(f)$. This controller FRF can also be obtained out of measurements. In theory, by using the closed loop system given in figure 4.1, the controller is given by

$$\frac{T(f)}{PS(f)} = C(f) \tag{7.21}$$

Here $T(f)$ is the complementary sensitivity function defined by (4.4) and $PS(f)$ is the process sensitivity function defined by

$$PS(f) = \frac{H(f)}{1 + C(f)H(f)} \tag{7.22}$$

Now observe the digital control system given in figure 6.1. The process sensitivity function can be obtained by

$$PS(f) = \frac{S_{ze}}{S_{zz}} = \frac{-IEI(f)H(f)DAC(f)}{1 + C(f)IEI(f)H(f)DAC(f)} \tag{7.23}$$

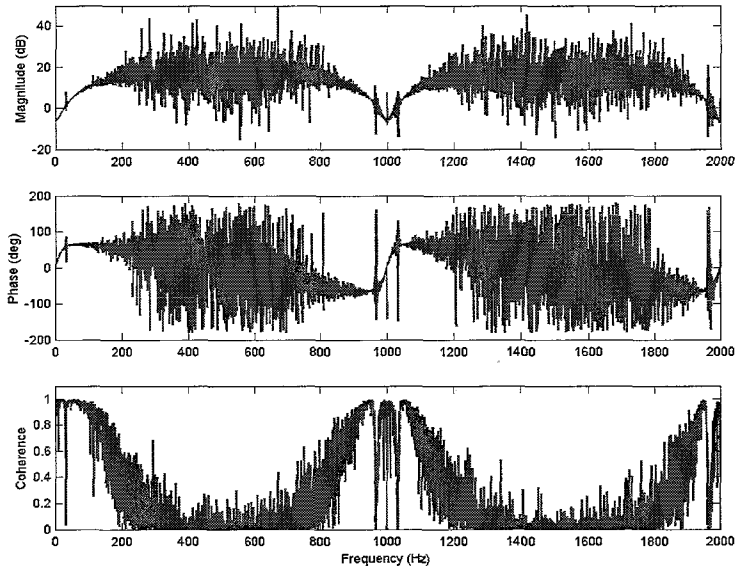


Figure 7.13: FRF and coherence of controller measurement for $f_s = 1000$ Hz

where $S_{ze}$ and $S_{zz}$ are given in Appendix B. Further by using (6.9) and $T(f) = -H_1(f)$ again relation (7.21) applies. The measurement result is given in figure 7.13 for $f_s = 1000$ Hz. For this measurement the same procedure is used as is described in section 4.2 and the results are obtained from 20 intervals of 100 Hz and 512 samples each. The corresponding frequency resolution is 0.25 Hz.

### 7.2.1 Conclusion Controller $C$

In figure 7.13, till the Nyquist frequency and besides the variance on the signal, the $PD$ control characteristic can be distinguished. For the whole FRF again the spectrum is folded around the Nyquist frequency and also the periodicity with $f_s$ appears. Although it is only demonstrated for $f_s = 1000$ Hz, the periodicity of the control characteristic is assumed to apply for every sampling frequency.

## 7.3 Process $H$

The third component of the open loop FRF, given by (6.13), is the FRF of process $H(f)$. This FRF can also be obtained from measurements. In theory, by using the closed loop system given in figure 4.1, the process is given by

$$\frac{PS(f)}{S(f)} = H(f) \tag{7.24}$$

Here $S(f)$ is the sensitivity function defined by (4.2) and $PS(f)$ is the process sensitivity function defined by (7.22). Now observe the digital control system given in figure 6.1. Here the ratio of the

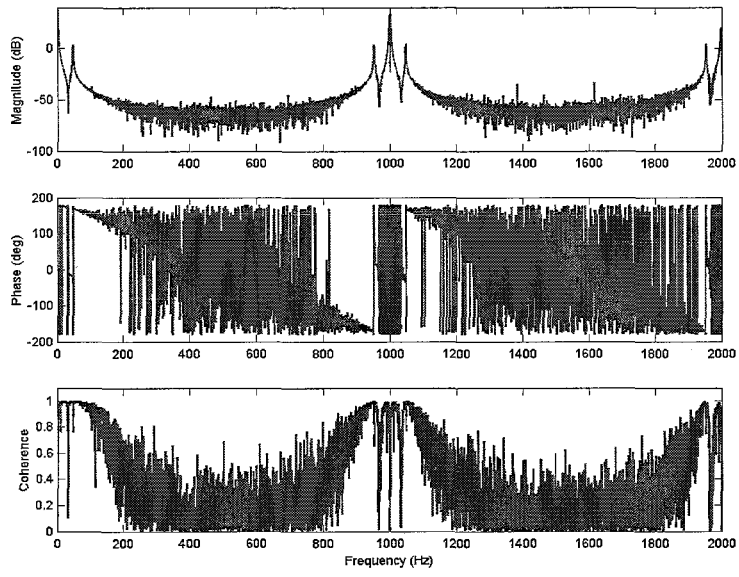


Figure 7.14: FRF and coherence of process measurement for $f_s = 1000$ Hz

process sensitivity function and sensitivity function results in

$$\frac{PS(f)}{S(f)} = -IEI(f)H(f)DAC(f) \tag{7.25}$$

As expected, the product of the ratio of the complementary sensitivity function and the process sensitivity function, given in (7.21), and the ratio of the process sensitivity function and sensitivity function, given in (7.25), equals the open loop FRF as given in (6.13).

The measurement result is given in figure 7.14 for $f_s = 1000$ Hz. For this measurement again the same procedure is used as is described in section 4.2 and again the results are obtained from 20 intervals of 100 Hz and 512 samples each. The corresponding frequency resolution is also 0.25 Hz.

### 7.3.1 Conclusion Process $H$

Observing figure 7.14, till the Nyquist frequency and besides the variance on the signal, the process is very clear and can be compared to the process given in figure 3.2. For the whole FRF again the spectrum is folded around the Nyquist frequency and also the periodicity with $f_s$ appears. Again it is assumed that this applies for every sampling frequency. When comparing the measured FRF of the process to the calculated FRF of (7.25) there is one clear difference. The behavior of the FRF of the DAC unit, as was derived in section 7.1, cannot be observed in the measured FRF. According to (7.25) there is a possibility that the FRF of the IEI unit cancels the behavior of the DAC unit. Therefore in the next section the IEI unit is discussed in more detail.

## 7.4 IEI unit

As is discussed in section 6.1 the IEI unit only counts the encoder lines produced by the incremental encoder. After a multiplier the output is given in radians according to (6.2). To investigate the dependency of different sampling frequencies, here the output in radians is measured, for $f_s = 2000$ Hz and $f_s = 1000$ Hz, inside dSpace while the masses are rotating at a constant velocity of 60 rad/s. The result for $f_s = 2000$ Hz is given in figure 7.15. Here the absolute position is given during 0.1 seconds repeatedly observed at regular time instants of 0.0005 seconds. This corresponds indeed to a sampling frequency of 2000 Hz. The corresponding increase of the angular position $\phi$ as function of time varies in this case between $\frac{8\pi}{1000}$ ($\approx 0.025$) and $\frac{11\pi}{1000}$ ($\approx 0.035$). The fact that the increase is not linear as function of time is due the oscillating flexibel bar between the two masses.

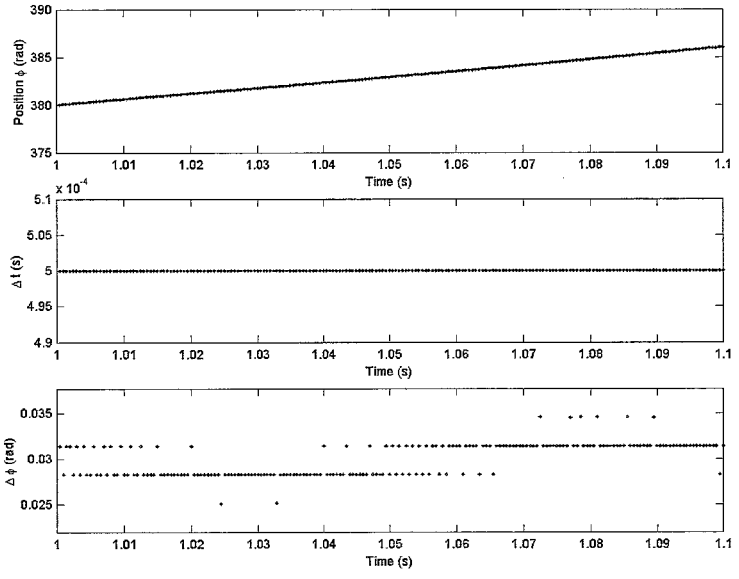


Figure 7.15: Encoder measurement with $f_s = 2000$ Hz for a constant velocity of 60 rad/s with the absolute position as function of time (top), sample period as function of time (middle) and increase of angular position as function of time (bottom)

Secondly the same procedure is followed for a sampling frequency of 1000 Hz. The result is given in figure 7.16. Here the sample period is constant 0.001 seconds and corresponds to the mentioned sampling frequency of 1000 Hz. The corresponding increase of the angular position as function of time varies is in this case between $\frac{17\pi}{1000}$ ($\approx 0.053$) and $\frac{21\pi}{1000}$ ($\approx 0.066$).

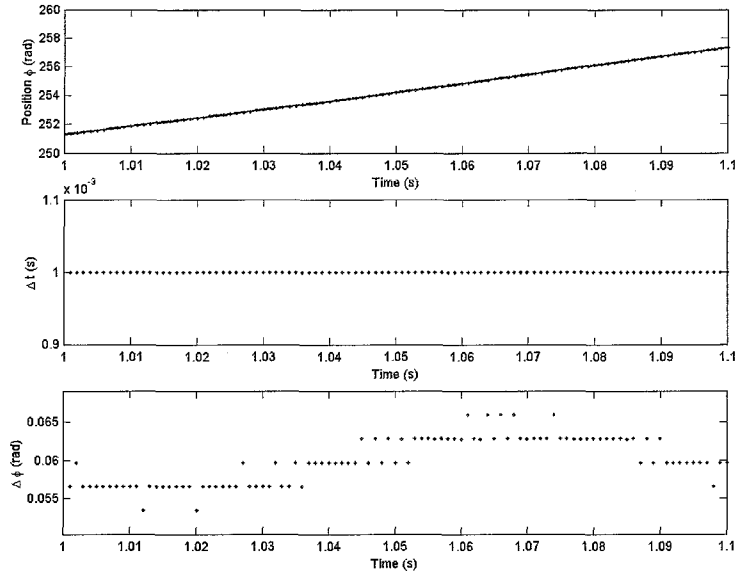


Figure 7.16: Encoder measurement with $f_s = 1000$ Hz for a constant velocity of 60 rad/s with the absolute position as function of time (top), sample period as function of time (middle) and increase of angular position as function of time (bottom)

### 7.4.1 Conclusion IEI unit

From the obtained results it can be concluded that inside the IEI unit every encoder line produced by the incremental encoder is counted. The sampling frequency dependency can be found in the time at which the counted number of encoder lines become available, but the sampling frequency does not influence the position value in time. This can be observed in the two time measurements where at $f_s = 2000$ Hz the position information is available at two times the position information at $f_s = 1000$ Hz. The consequence is that the corresponding value for the position at $f_s = 2000$ Hz is twice as low as the corresponding value for the position at $f_s = 1000$ Hz. It should be noted that at the used constant prescribed velocity of 60 radians per second the counted position becomes critical when a dSpace sampling frequency of 20 kHz is reached.

Since here a maximum sampling frequency of 2000 Hz is used it can be concluded that the incremental encoder together with the IEI unit is nothing else than digitizing the angular position, as indeed was stated in section 6.1. As a consequence the possibility, as stated in section 7.3.1, that the frequency domain behavior of the IEI unit could cancel the frequency domain behavior of DAC unit is unlikely.

# Chapter 8

# Conclusions and Recommendations

In this report the effect of the sampling frequency of a digital controller on the open loop FRF of a controlled fourth order system was investigated. Therefore first the control system and the identification by measurements was discussed. Secondly measurement methods of the open loop FRF were given in continuous time. Since in the measurement results aliasing effects were observed it was asumed that the continuous time representation of the controlled system was not appropriate to use here. Therefore, before trying to explain the measurement results and the sampling frequency dependency, first the open loop FRF was recalculated for a mixed continuous and discrete time system with the interface included. The newly obtained open loop FRF consists besides the FRF of the controller and process also of a FRF of a digital to analog converter and a FRF of an incremental encoder interface.

Summarized, the incremental encoder interface only represents the absolute angular position by a digital variant. For the observed system configuration in this report no sampling frequency dependency can be found on the encoder position value. For the controller FRF as well as for the process FRF, only a periodicity, with a period of one sampling frequency, was obtained of respectively the control characteristic and the fourth order system characteristic and its aliased similarity. Finally, for the digital to analog converter, a zero order hold was included. The corresponding transfer function, with a sampling frequency dependency, affects both the magnitude and phase and is appropriate to describe the frequency domain behavior, as was demonstrated. But, in spite of the fact that the four considered components of the measured open loop FRF, and its sampling frequency dependency, were all identified separately, the overall system behavior can not be covered. So, it is concluded that with these four components the measured open loop FRF system behavior can not be described sufficient.

Finally, it is possible that the interface, presented in this report, is not completely representative or that the sampling frequency dependency of the interface is not identified carefully. For further analysis, based on the presented interface description, most attention should be paid to the incremental encoder interface and its frequency domain behavior since in this report only the time domain was considered. Another aspect that still has to be investigated, in more detail, is the additional phase lag obtained at the interface output. Finally, also the system behavior should be investigated for different reference trajectory velocities. After all, in any case, when using excitation signals which exceed the Nyquist frequency, special attention should be paid to the importance of the coherence measurement as was demonstrated.

# Appendix A

# Closed Loop Power Spectral Density Functions

## A.1 Auto Spectral Density Function $S_{ww}(f)$

Observe $W(f)$. Premultiplying of $W(f)$ with the complex conjugate of $W(f)$ and $\frac{1}{T}$ gives

$$S_{ww}(f) = \frac{1}{T} W^*(f) W(f) \tag{A.1}$$

## A.2 Auto Spectral Density Function $S_{uu}(f)$

Observe $U(f)$. The closed loop equation for $U(f)$ is given by

$$U(f) = \frac{1}{1 + C(f)H(f)} \Big( W(f) + C(f)R(f) - C(f)M(f) - C(f)H(f)N(f) \Big) \tag{A.2}$$

Premultiplying with the complex conjugate of $U(f)$ and $\frac{1}{T}$ gives

$$\frac{1}{T} U^*(f) U(f) = \frac{1}{1 + C(f)H(f)} \frac{1}{T} \Big( U^*(f) W(f) + C(f) U^*(f) R(f) - C(f) U^*(f) M(f) - C(f) H(f) U^*(f) N(f) \Big) \tag{A.3}$$

with the complex conjugate of $U(f)$ given by

$$U^*(f) = \frac{1}{1 + C^*(f)H^*(f)} \Big( W^*(f) + C^*(f)R^*(f) - C^*(f)M^*(f) - C^*(f)H^*(f)N^*(f) \Big) \tag{A.4}$$

follows

$$\begin{aligned}\frac{1}{T}U^*(f)U(f)| = &\frac{1}{1+C^*(f)H^*(f)}\frac{1}{1+C(f)H(f)}\frac{1}{T}\\ &\Big(\Big[W^*(f)+C^*(f)R^*(f)-C^*(f)M^*(f)-C^*(f)H^*(f)N^*(f)\Big]W(f)\\ &+\Big[W^*(f)+C^*(f)R^*(f)-C^*(f)M^*(f)-C^*(f)H^*(f)N^*(f)\Big]C(f)R(f)\\ &-\Big[W^*(f)+C^*(f)R^*(f)-C^*(f)M^*(f)-C^*(f)H^*(f)N^*(f)\Big]C(f)M(f)\\ &-\Big[W^*(f)+C^*(f)R^*(f)-C^*(f)M^*(f)-C^*(f)H^*(f)N^*(f)\Big]C(f)H(f)N(f)\Big)\end{aligned} \tag{A.5}$$

with uncorrelated inputs and in terms of spectral density functions follows

$$\begin{aligned}S_{uu}(f) = &\frac{1}{1+C^*(f)H^*(f)}\frac{1}{1+C(f)H(f)}\\ &\Big(S_{ww}(f)+C^*(f)C(f)S_{rr}(f)+C^*(f)C(f)S_{mm}(f)+C^*(f)C(f)H^*(f)H(f)S_{nn}(f)\Big)\end{aligned} \tag{A.6}$$

## A.3 Cross Spectral Density Function $S_{wu}(f)$

Observe $U(f)$ as given by (A.2). Premultiplying with the complex conjugate of $W(f)$ and $\frac{1}{T}$ gives

$$\frac{1}{T}W^*(f)U(f) = \frac{1}{1+C(f)H(f)}\frac{1}{T}\Big(W^*(f)W(f)+C(f)W^*(f)R(f)-C(f)W^*(f)M(f)-C(f)H(f)W^*(f)N(f)\Big) \tag{A.7}$$

with uncorrelated inputs and in terms of spectral density functions follows

$$S_{wu}(f) = \frac{1}{1+C(f)H(f)}S_{ww}(f) \tag{A.8}$$

## A.4 Cross Spectral Density Function $S_{uw}(f)$

Observe $W(f)$. Premultiplying of $W(f)$ with the complex conjugate of $U(f)$, corresponding to (A.4), and $\frac{1}{T}$ gives

$$\begin{aligned}\frac{1}{T}U^*(f)W(f) = &\frac{1}{1+C^*(f)H^*(f)}\frac{1}{T}\Big(W^*(f)W(f)+C^*(f)R^*(f)W(f)\\ &-C^*(f)M^*(f)W(f)-C^*(f)H^*(f)N^*(f)W(f)\Big)\end{aligned} \tag{A.9}$$

with uncorrelated inputs and in terms of spectral density functions follows

$$S_{uw}(f) = \frac{1}{1+C^*(f)H^*(f)}S_{ww}(f) \tag{A.10}$$

This also corresponds with

$$S_{uw}(f) = S_{wu}(-f) = S^*_{wu}(f) \tag{A.11}$$

## A.5 Auto Spectral Density Function $S_{vv}(f)$

Observe $V(f)$. The closed loop equation for $V(f)$ is given by

$$V(f) = \frac{1}{1+C(f)H(f)}\Big(C(f)R(f) - C(f)M(f) - C(f)H(f)N(f) - C(f)H(f)W(f)\Big) \tag{A.12}$$

Premultiplying with the complex conjugate of $V(f)$ and $\frac{1}{T}$ gives

$$\frac{1}{T}V^*(f)V(f) = \frac{1}{1+C(f)H(f)}\frac{1}{T}\Big(C(f)V^*(f)R(f) - C(f)V^*(f)M(f) - C(f)H(f)V^*(f)N(f) - C(f)H(f)V^*(f)W(f)\Big) \tag{A.13}$$

with the complex conjugate of $V(f)$ given by

$$V^*(f) = \frac{1}{1+C^*(f)H^*(f)}\Big(C^*(f)R^*(f) - C^*(f)M^*(f) - C^*(f)H^*(f)N^*(f) - C^*(f)H^*(f)W^*(f)\Big) \tag{A.14}$$

follows

$$\begin{aligned}\frac{1}{T}V^*(f)V(f)| = {} & \frac{1}{1+C^*(f)H^*(f)}\frac{1}{1+C(f)H(f)}\frac{1}{T} \\ & \Big(\Big[C^*(f)R^*(f) - C^*(f)M^*(f) - C^*(f)H^*(f)N^*(f) - C^*(f)H^*(f)W^*(f)\Big]C(f)R(f) \\ & -\Big[C^*(f)R^*(f) - C^*(f)M^*(f) - C^*(f)H^*(f)N^*(f) - C^*(f)H^*(f)W^*(f)\Big]C(f)M(f) \\ & -\Big[C^*(f)R^*(f) - C^*(f)M^*(f) - C^*(f)H^*(f)N^*(f) - C^*(f)H^*(f)W^*(f)\Big]C(f)H(f)N(f) \\ & -\Big[C^*(f)R^*(f) - C^*(f)M^*(f) - C^*(f)H^*(f)N^*(f) - C^*(f)H^*(f)W^*(f)\Big]C(f)H(f)W(f)\Big)\end{aligned} \tag{A.15}$$

with uncorrelated inputs and in terms of spectral density functions follows

$$S_{vv}(f) = \frac{1}{1+C^*(f)H^*(f)}\frac{1}{1+C(f)H(f)}\Big(C^*(f)C(f)S_{rr}(f) + C^*(f)C(f)S_{mm}(f) + C^*(f)C(f)H^*(f)H(f)S_{nn}(f) + C^*(f)C(f)H^*(f)H(f)S_{ww}(f)\Big) \tag{A.16}$$

## A.6 Cross Spectral Density Function $S_{wv}(f)$

Observe $V(f)$ as given by (A.12). Premultiplying with the complex conjugate of $W(f)$ and with $\frac{1}{T}$ gives

$$\frac{1}{T}W^*(f)V(f) = \frac{1}{1+C(f)H(f)}\frac{1}{T}\Big(C(f)W^*(f)R(f) - C(f)W^*(f)M(f) - C(f)H(f)W^*(f)N(f) - C(f)H(f)W^*(f)W(f)\Big) \tag{A.17}$$

with uncorrelated inputs and in terms of spectral density functions follows

$$S_{wv}(f) = -\frac{C(f)H(f)}{1+C(f)H(f)}S_{ww}(f) \tag{A.18}$$

## A.7 Cross Spectral Density Function $S_{vw}(f)$

Observe $W(f)$. Premultiplying of $W(f)$ with the complex conjugate of $V(f)$, corresponding to (A.14), and $\frac{1}{T}$ gives

$$\frac{1}{T}V^*(f)W(f) = \frac{1}{1+C^*(f)H^*(f)}\frac{1}{T}\Big(C^*(f)R^*(f)W(f) - C^*(f)M^*(f)W(f) - C^*(f)H^*(f)N^*(f)W(f) - C^*(f)H^*(f)W^*(f)W(f)\Big) \tag{A.19}$$

with uncorrelated inputs and in terms of spectral density functions follows

$$S_{vw}(f) = -\frac{C^*(f)H^*(f)}{1+C^*(f)H^*(f)}S_{ww}(f) \tag{A.20}$$

This also corresponds with

$$S_{vw}(f) = S_{wv}(-f) = S^*_{wv}(f) \tag{A.21}$$

# Appendix B

# Implemented Closed Loop Power Spectral Density Functions

## B.1 Auto Spectral Density Function $S_{zz}(f)$

Observe $Z(f)$. The open loop equation for $Z(f)$ is given by

$$Z(f) = DAC(f)ADC(f)W(f) \tag{B.1}$$

Premultiplying of $Z(f)$ with the complex conjugate of $Z(f)$ and $\frac{1}{T}$ gives

$$\frac{1}{T}Z^*(f)Z(f) = \frac{1}{T}DAC(f)ADC(f)Z^*(f)W(f) \tag{B.2}$$

with the complex conjugate of $Z(f)$ given by

$$Z^*(f) = DAC^*(f)ADC^*(f)W^*(f) \tag{B.3}$$

follows in terms of spectral density functions

$$S_{zz}(f) = |DAC(f)|^2|ADC(f)|^2 S_{ww}(f) \tag{B.4}$$

## B.2 Auto Spectral Density Function $S_{uu}(f)$

Observe $U(f)$. The closed loop equation for $U(f)$ is given by

$$U(f) = \frac{1}{1 + DAC(f)C(f)IEI(f)H(f)}\Big( DAC(f)W_k + DAC(f)C(f)R_k - DAC(f)C(f)IEI(f)M(f) - DAC(f)C(f)IEI(f)H(f)N(f)\Big) \tag{B.5}$$

Here $W_k$ and $R_k$ are discrete inputs. For an analog input the discrete values has to be sent through a ADC unit. This results in

$$\begin{aligned} W_k &= ADC(f)W(f) \\ R_k &= ADC(f)R(f) \end{aligned} \tag{B.6}$$

The closed loop equation of (B.5) becomes

$$U(f) = \frac{1}{1 + DAC(f)C(f)IEI(f)H(f)} \Big( DAC(f)ADC(f)W(f) + DAC(f)ADC(f)C(f)R(f) - DAC(f)C(f)IEI(f)M(f) - DAC(f)C(f)IEI(f)H(f)N(f) \Big) \quad \text{(B.7)}$$

Premultiplying with the complex conjugate of $U(f)$ and $\frac{1}{T}$ gives

$$\frac{1}{T}U^*(f)U(f) = \frac{1}{T}\frac{1}{1 + DAC(f)C(f)IEI(f)H(f)} \Big( DAC(f)ADC(f)U^*(f)W(f) + DAC(f)ADC(f)C(f)U^*(f)R(f) - DAC(f)C(f)IEI(f)U^*(f)M(f) - DAC(f)C(f)IEI(f)H(f)U^*(f)N(f) \Big) \quad \text{(B.8)}$$

with the complex conjugate of $U(f)$ given by

$$U^*(f) = \frac{1}{1 + DAC^*(f)C^*(f)IEI^*(f)H^*(f)} \Big( DAC^*(f)ADC^*(f)W^*(f) + DAC^*(f)ADC^*(fC^*(f)R^*(f) - DAC^*(f)C^*(f)IEI^*(f)M^*(f) - DAC^*(f)C^*(f)IEI^*(f)H^*(f)N^*(f) \Big) \quad \text{(B.9)}$$

follows

$$\begin{aligned}
\frac{1}{T}U^*(f)U(f) = {} & \frac{1}{1 + DAC^*(f)C^*(f)IEI^*(f)H^*(f)} \frac{1}{1 + DAC(f)C(f)IEI(f)H(f)} \frac{1}{T} \\
& \Big( \Big[ ADC^*(f)DAC^*(f)W^*(f) + ADC^*(f)DAC^*(f)C^*(f)R^*(f) - DAC^*(f)C^*(f)IEI^*(f)M^*(f) \\
& \quad - DAC^*(f)C^*(f)IEI^*(f)H^*(f)N^*(f) \Big] ADC(f)DAC(f)W(f) \\
& + \Big[ ADC^*(f)DAC^*(f)W^*(f) + ADC^*(f)DAC^*(f)C^*(f)R^*(f) - DAC^*(f)C^*(f)IEI^*(f)M^*(f) \\
& \quad - DAC^*(f)C^*(f)IEI^*(f)H^*(f)N^*(f) \Big] ADC(f)DAC(f)C(f)R(f) \\
& - \Big[ ADC^*(f)DAC^*(f)W^*(f) + ADC^*(f)DAC^*(f)C^*(f)R^*(f) - DAC^*(f)C^*(f)IEI^*(f)M^*(f) \\
& \quad - DAC^*(f)C^*(f)IEI^*(f)H^*(f)N^*(f) \Big] DAC(f)C(f)IEI(f)M(f) \\
& - \Big[ ADC^*(f)DAC^*(f)W^*(f) + ADC^*(f)DAC^*(f)C^*(f)R^*(f) - DAC^*(f)C^*(f)IEI^*(f)M^*(f) \\
& \quad - DAC^*(f)C^*(f)IEI^*(f)H^*(f)N^*(f) \Big] DAC(f)C(f)IEI(f)H(f)N(f) \Big)
\end{aligned} \quad \text{(B.10)}$$

with uncorrelated inputs and in terms of spectral density functions follows

$$\begin{aligned}
S_{uu}(f) = {} & \frac{1}{1 + DAC^*(f)C^*(f)IEI^*(f)H^*(f)} \frac{1}{1 + DAC(f)C(f)IEI(f)H(f)} \\
& \Big( |ADC(f)|^2 |DAC(f)|^2 S_{ww}(f) + |ADC(f)|^2 |DAC(f)|^2 |C(f)|^2 S_{rr}(f) + \\
& \quad |DAC(f)|^2 |C(f)|^2 |IEI(f)|^2 S_{mm}(f) + |DAC(f)|^2 |C(f)|^2 |IEI(f)|^2 |H(f)|^2 S_{nn}(f) \Big)
\end{aligned} \quad \text{(B.11)}$$

## B.3 Cross Spectral Density Function $S_{zu}(f)$

Observe $U(f)$ as given by (B.7). Premultiplying with the complex conjugate of $Z(f)$ and $\frac{1}{T}$ gives

$$\frac{1}{T}Z^*(f)U(f) = \frac{1}{1+DAC(f)C(f)IEI(f)H(f)}\frac{1}{T}\Big(ADC(f)DAC(f)Z^*(f)W(f)+ADC(f)C(f)DAC(f)Z^*(f)R(f) - DAC(f)C(f)IEI(f)Z^*(f)M(f) - DAC(f)C(f)IEI(f)H(f)Z^*(f)N(f)\Big) \quad \text{(B.12)}$$

with the complex conjugate of $Z(f)$ given by (B.3) follows

$$\begin{aligned}\frac{1}{T}U^*(f)U(f) = {} & \frac{1}{1+DAC(f)C(f)IEI(f)H(f)}\frac{1}{T} \\ & \Big(\Big[ADC^*(f)DAC^*(f)W^*(f)\Big]ADC(f)DAC(f)W(f) \\ & +\Big[ADC^*(f)DAC^*(f)W^*(f)\Big]ADC(f)C(f)DAC(f)R(f) \\ & -\Big[ADC^*(f)DAC^*(f)W^*(f)\Big]DAC(f)C(f)IEI(f)M(f) \\ & -\Big[ADC^*(f)DAC^*(f)W^*(f)\Big]DAC(f)C(f)IEI(f)H(f)N(f)\Big)\end{aligned} \quad \text{(B.13)}$$

with uncorrelated inputs and in terms of spectral density functions follows

$$S_{zu}(f) = \frac{|ADC(f)|^2|DAC(f)|^2}{1+DAC(f)C(f)IEI(f)H(f)}S_{ww}(f) \quad \text{(B.14)}$$

## B.4 Cross Spectral Density Function $S_{uz}(f)$

Observe $Z(f)$ as given by (B.1). Premultiplying with the complex conjugate of $U(f)$ and $\frac{1}{T}$ gives

$$\frac{1}{T}U^*(f)Z(f) = \frac{1}{T}\Big(ADC(f)DAC(f)U^*(f)W(f)\Big) \quad \text{(B.15)}$$

with the complex conjugate of $U(f)$ given by (B.9) follows

$$\begin{aligned}\frac{1}{T}U^*(f)Z(f) = {} & \frac{1}{1+DAC(f)C(f)IEI(f)H(f)}\frac{1}{T}\Big(\Big[ADC^*(f)DAC^*(f)W^*(f)+ADC^*(f)DAC^*(f)C^*(f)R^*(f) \\ & -DAC^*(f)C^*(f)IEI^*(f)M^*(f)-DAC^*(f)C^*(f)IEI^*(f)H^*(f)N^*(f)\Big]ADC(f)DAC(f)W(f)\Big)\end{aligned} \quad \text{(B.16)}$$

with uncorrelated inputs and in terms of spectral density functions follows

$$S_{uz}(f) = \frac{|ADC(f)|^2|DAC(f)|^2}{1+DAC^*(f)C^*(f)IEI^*(f)H^*(f)}S_{ww}(f) \quad \text{(B.17)}$$

This also corresponds with

$$S_{uz}(f) = S_{zu}(-f) = S^*_{zu}(f) \quad \text{(B.18)}$$

## B.5 Auto Spectral Density Function $S_{vv}(f)$

Observe $V(f)$. $V(f)$ is given by

$$V(f) = DAC(f)V_k \tag{B.19}$$

The closed loop equation for $V_k$ is given by

$$V_k = \frac{1}{1 + C(f)IEI(f)H(f)DAC(f)} \Big( C(f)R_k - C(f)IEI(f)M(f) \\ - C(f)IEI(f)H(f)N(f) - C(f)IEI(f)H(f)DAC(f)W_k \Big) \tag{B.20}$$

With relation (B.6) and (B.19) follows

$$V(f) = \frac{DAC(f)}{1 + C(f)IEI(f)H(f)DAC(f)} \Big( ADC(f)C(f)R(f) - C(f)IEI(f)M(f) \\ - C(f)IEI(f)H(f)N(f) - ADC(f)C(f)IEI(f)H(f)DAC(f)W(f) \Big) \tag{B.21}$$

and premultiplying with the complex conjugate of $V(f)$ and $\frac{1}{T}$ gives

$$\frac{1}{T}V^*(f)V(f) = \frac{1}{T}\frac{DAC(f)}{1 + C(f)IEI(f)H(f)DAC(f)} \Big( ADC(f)C(f)V^*(f)R(f) - C(f)IEI(f)V^*(f)M(f) \\ - C(f)IEI(f)H(f)V^*(f)N(f) - ADC(f)C(f)IEI(f)H(f)DAC(f)W^*(f)W(f) \Big) \tag{B.22}$$

with the complex conjugate of $V(f)$ given by

$$V^*(f) = \frac{DAC^*(f)}{1 + C^*(f)IEI^*(f)H^*(f)DAC^*(f)} \Big( ADC^*(f)C^*(f)R^*(f) - C^*(f)IEI^*(f)M^*(f) \\ - C^*(f)IEI^*(f)H^*(f)N^*(f) - ADC^*(f)C^*(f)IEI^*(f)H^*(f)DAC^*(f)W^*(f) \Big) \tag{B.23}$$

follows

$$\begin{aligned} \frac{1}{T}V^*(f)V(f) = \frac{1}{T}\frac{DAC^*(f)}{1 + C^*(f)IEI^*(f)H^*(f)DAC^*(f)}\frac{DAC(f)}{1 + C(f)IEI(f)H(f)DAC(f)} \\ \Big( \Big[ ADC^*(f)C^*(f)R^*(f) - C^*(f)IEI^*(f)M^*(f) - C^*(f)IEI^*(f)H^*(f)N^*(f) \\ -ADC^*(f)C^*(f)IEI^*(f)H^*(f)DAC^*(f)W^*(f) \Big] ADC(f)C(f)R(f) \\ - \Big[ ADC^*(f)C^*(f)R^*(f) - C^*(f)IEI^*(f)M^*(f) - C^*(f)IEI^*(f)H^*(f)N^*(f) \\ -ADC^*(f)C^*(f)IEI^*(f)H^*(f)DAC^*(f)W^*(f) \Big] C(f)IEI(f)M(f) \\ - \Big[ ADC^*(f)C^*(f)R^*(f) - C^*(f)IEI^*(f)M^*(f) - C^*(f)IEI^*(f)H^*(f)N^*(f) \\ -ADC^*(f)C^*(f)IEI^*(f)H^*(f)DAC^*(f)W^*(f) \Big] C(f)IEI(f)H(f)N(f) \\ - \Big[ ADC^*(f)C^*(f)R^*(f) - C^*(f)IEI^*(f)M^*(f) - C^*(f)IEI^*(f)H^*(f)N^*(f) \\ -ADC^*(f)C^*(f)IEI^*(f)H^*(f)DAC^*(f)W^*(f) \Big] ADC(f)C(f)IEI(f)H(f)DAC(f)W(f) \Big) \end{aligned} \tag{B.24}$$

with uncorrelated inputs and in terms of spectral density functions follows

$$S_{vv}(f) = \frac{DAC^*(f)}{1 + C^*(f)IEI^*(f)H^*(f)DAC^*(f)} \frac{DAC(f)}{1 + C(f)IEI(f)H(f)DAC(f)}$$
$$\Big( |ADC(f)|^2|C(f)|^2 S_{rr}(f) + |C(f)|^2|IEI(f)|^2 S_{mm}(f) + |C(f)|^2|IEI(f)|^2|H(f)|^2 S_{nn}(f) +$$
$$|ADC(f)|^2|C(f)|^2|IEI(f)|^2|H(f)|^2|DAC(f)|^2 S_{ww}(f) \Big) \quad \text{(B.25)}$$

## B.6 Cross Spectral Density Function $S_{zv}(f)$

Observe $V(f)$ as given by (B.21). Premultiplying with the complex conjugate of $Z(f)$ and with $\frac{1}{T}$ gives

$$\frac{1}{T} Z^*(f)V(f) = \frac{DAC(f)}{1 + C(f)IEI(f)H(f)DAC(f)} \frac{1}{T} \Big( ADC(f)C(f)Z^*(f)R(f) - C(f)IEI(f)Z^*(f)M(f)$$
$$- C(f)IEI(f)H(f)Z^*(f)N(f) - ADC(f)C(f)IEI(f)H(f)DAC(f)Z^*(f)W(f) \Big) \quad \text{(B.26)}$$

with the complex conjugate of $Z(f)$ given by (B.3) follows

$$\frac{1}{T} Z^*(f)V(f) = \frac{DAC(f)}{1 + DAC(f)C(f)IEI(f)H(f)} \frac{1}{T}$$
$$\Big( \Big[ ADC^*(f)DAC^*(f)W^*(f) \Big] ADC(f)C(f)R(f)$$
$$- \Big[ ADC^*(f)DAC^*(f)W^*(f) \Big] C(f)IEI(f)M(f) \quad \text{(B.27)}$$
$$- \Big[ ADC^*(f)DAC^*(f)W^*(f) \Big] C(f)IEI(f)H(f)N(f)$$
$$- \Big[ ADC^*(f)DAC^*(f)W^*(f) \Big] ADC(f)C(f)IEI(f)H(f)DAC(f)W(f) \Big)$$

with uncorrelated inputs and in terms of spectral density functions follows

$$S_{zv}(f) = \frac{-C(f)IEI(f)H(f)DAC(f)}{1 + C(f)IEI(f)H(f)DAC(f)} |DAC(f)|^2|ADC(f)|^2 S_{ww}(f) \quad \text{(B.28)}$$

## B.7 Cross Spectral Density Function $S_{vz}(f)$

Observe $Z(f)$ as given by (B.1). Premultiplying with the complex conjugate of $V(f)$ and $\frac{1}{T}$ gives

$$\frac{1}{T} V^*(f)Z(f) = \frac{1}{T} \Big( ADC(f)DAC(f)V^*(f)W(f) \Big) \quad \text{(B.29)}$$

with the complex conjugate of $V(f)$ given by (B.23) follows

$$\frac{1}{T} V^*(f)Z(f) = \frac{DAC^*(f)}{1 + DAC^*(f)C^*(f)IEI^*(f)H^*(f)} \frac{1}{T}$$
$$\Big( \Big[ ADC^*(f)C^*(f)R^*(f) - C^*(f)IEI^*(f)M^*(f) - C^*(f)IEI^*(f)H^*(f)N^*(f) \quad \text{(B.30)}$$
$$- ADC^*(f)C^*(f)IEI^*(f)H^*(f)DAC^*(f)W^*(f) \Big] ADC(f)DAC(f)W(f) \Big)$$

with uncorrelated inputs and in terms of spectral density functions follows

$$S_{vz}(f) = \frac{-DAC^*(f)C^*(f)IEI^*(f)H^*(f)}{1+C^*(f)IEI^*(f)H^*(f)DAC^*(f)}|ADC(f)|^2|DAC|^2 S_{ww}(f) \tag{B.31}$$

This also corresponds with

$$S_{vz}(f) = S_{zv}(-f) = S^*_{zv}(f) \tag{B.32}$$

## B.8 Auto Spectral Density Function $S_{ze}(f)$

Observe $E(f)$. $E(f)$ is given by

$$E(f) = DAC(f)E_k \tag{B.33}$$

The closed loop equation for $E_k$ is given by

$$E_k = \frac{1}{1+C(f)IEI(f)H(f)DAC(f)}\Big(R_k - IEI(f)M(f) - IEI(f)H(f)N(f) - IEI(f)H(f)DAC(f)W_k\Big) \tag{B.34}$$

With relation (B.6) and (B.33) follows

$$E(f) = \frac{DAC(f)}{1+C(f)IEI(f)H(f)DAC(f)}\Big(ADC(f)R(f) - IEI(f)M(f) - IEI(f)H(f)N(f) - ADC(f)IEI(f)H(f)DAC(f)W(f)\Big) \tag{B.35}$$

and premultiplying with the complex conjugate of $Z(f)$ and $\frac{1}{T}$ gives

$$\frac{1}{T}Z^*(f)E(f) = \frac{DAC(f)}{1+C(f)IEI(f)H(f)DAC(f)}\frac{1}{T}\Big(ADC(f)Z^*(f)R(f) - IEI(f)Z^*(f)M(f) - IEI(f)H(f)Z^*(f)N(f) - ADC(f)IEI(f)H(f)DAC(f)Z^*(f)W(f)\Big) \tag{B.36}$$

with the complex conjugate of $Z(f)$ given by (B.3) follows

$$\begin{aligned}\frac{1}{T}Z^*(f)E(f) = \frac{DAC(f)}{1+DAC(f)C(f)IEI(f)H(f)}\frac{1}{T}\\ \Big(\Big[ADC^*(f)DAC^*(f)W^*(f)\Big]ADC(f)R(f)\\ -\Big[ADC^*(f)DAC^*(f)W^*(f)\Big]IEI(f)M(f)\\ -\Big[ADC^*(f)DAC^*(f)W^*(f)\Big]IEI(f)H(f)N(f)\\ -\Big[ADC^*(f)DAC^*(f)W^*(f)\Big]ADC(f)IEI(f)H(f)DAC(f)W(f)\Big)\end{aligned} \tag{B.37}$$

with uncorrelated inputs and in terms of spectral density functions follows

$$S_{ze}(f) = \frac{-IEI(f)H(f)DAC(f)}{1+C(f)IEI(f)H(f)DAC(f)}|DAC(f)|^2|ADC(f)|^2 S_{ww}(f) \tag{B.38}$$

# Appendix C

# Sensitivity and Complementary Sensitivity Measurement Results

## C.1 Sensitivity Measurement

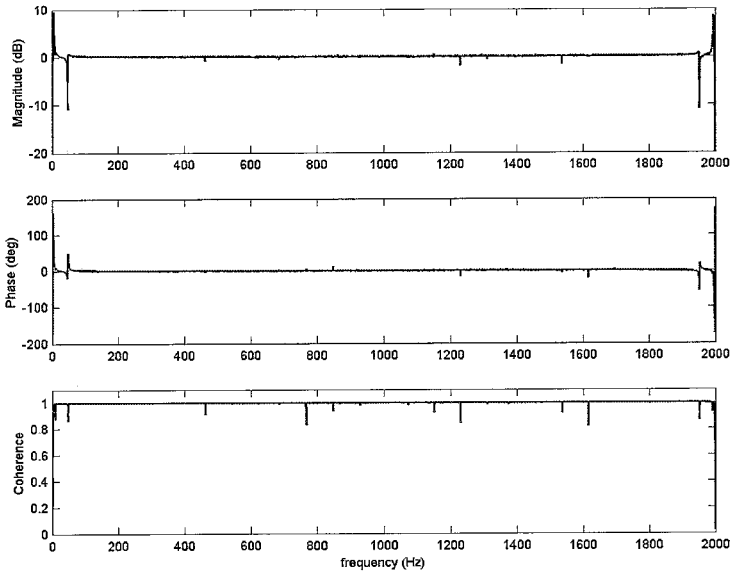


Figure C.1: Sensitivity measurement for $f_s = 2000$ Hz

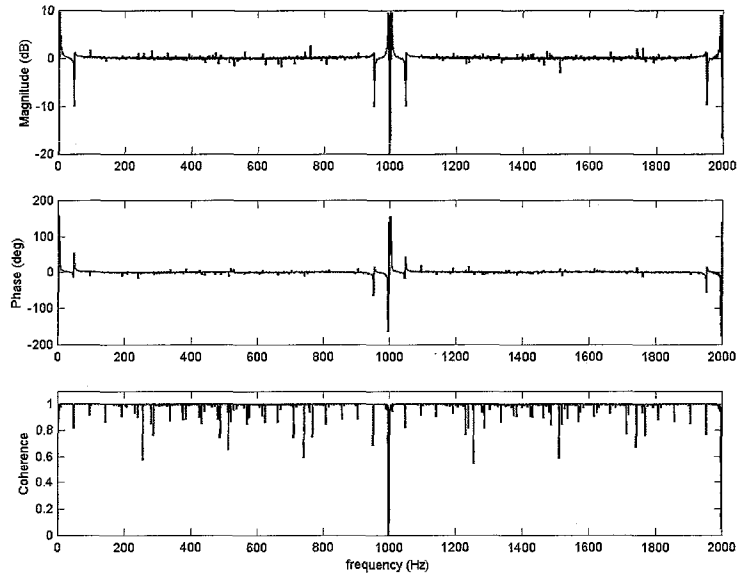


Figure C.2: Sensitivity measurement for $f_s = 1000$ Hz

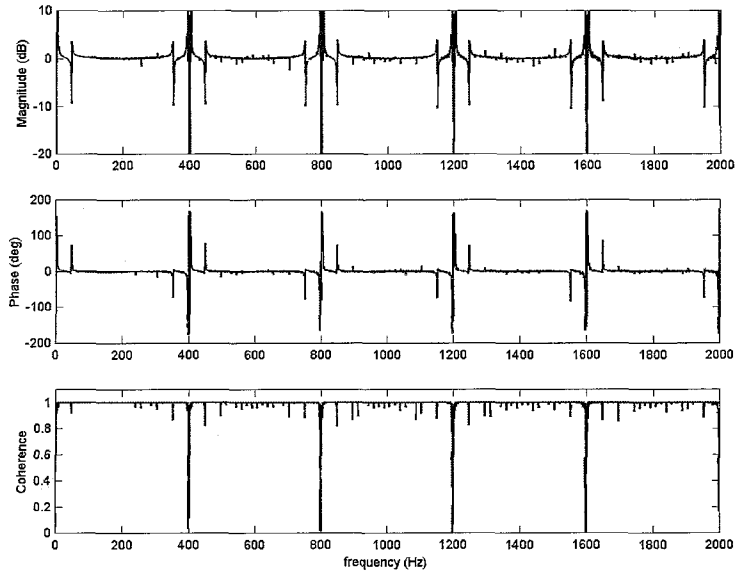


Figure C.3: Sensitivity measurement for $f_s = 400$ Hz

## C.2 Complementary Sensitivity Measurement

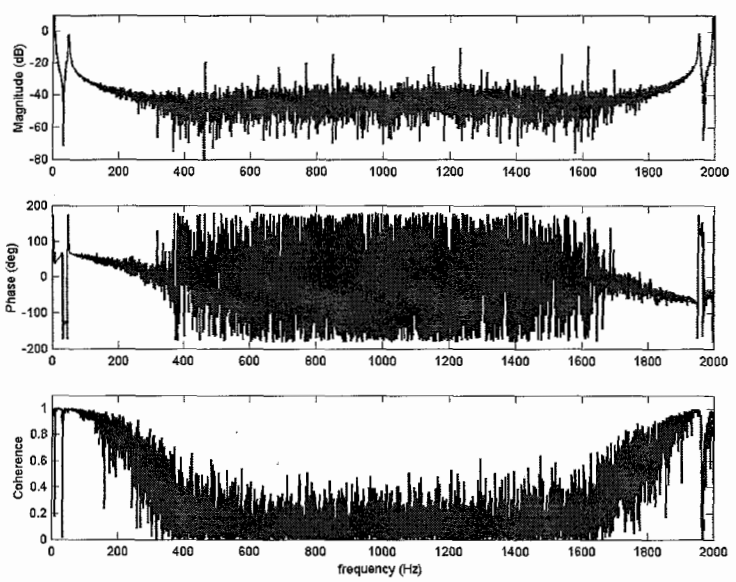


Figure C.4: Complementary sensitivity measurement for $f_s = 2000$ Hz

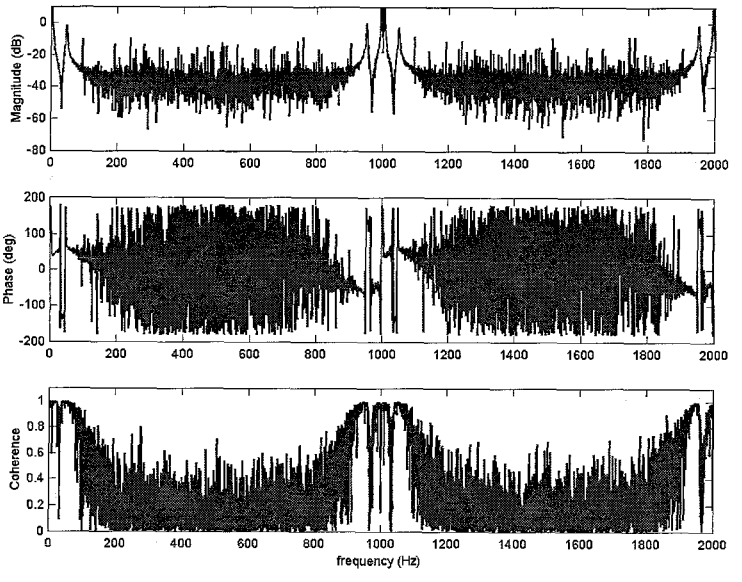


Figure C.5: Complementary sensitivity measurement for $f_s = 1000$ Hz

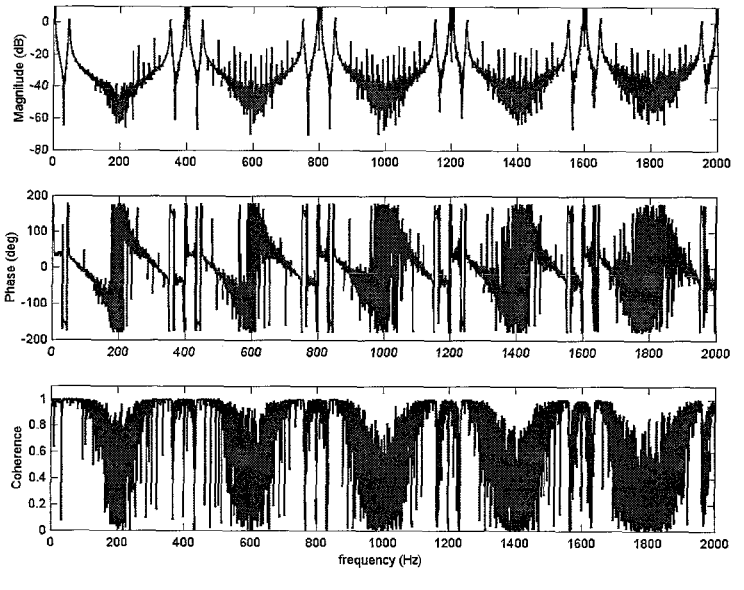


Figure C.6: Complementary sensitivity measurement for $f_s = 400$ Hz

# Bibliography


[1] J. S. Bendat and A. G. Piersol, "*Random Data: Analysis and Measurement Procedures,*" Second Edition, A Wiley-Intersience Publication, New York, 1986, ISBN 0-471-04000-2

[2] A. de Kraker, "*A Numerical-Experimental Approach in Structural Dynamics,*" Eindhoven Universitiy of Technology, Department of Mechanical Engineering, Section Engineering Dynamics, Lecture Notes 4784, May 2000

[3] J. Boot, "*Frequency Response Measurement in Closed Loop: Brushing Up Our Knowledge,*" Internship Report, Eindhoven Universitiy of Technology, Section Control Systems Technology, Reportnumber 2003.59, April 2003

[4] DS1102 DSP Controller Board, "*RTI Reference,*" september 1999

[5] G. F. Franklin and J. D. Powell, "*Digital Control of Dynamic Systems,*" Addison-Wesley Publishing Company, 1980. ISBN 0-201-02891-3

[6] M. J. Nieuwenhuizen, "*Quality of Open Loop Frequency Response Function Measurements in Servo Systems,*" Internship Report, Eindhoven Universitiy of Technology, Section Control Systems Technology, Reportnumber 2003.112, December 2003

[7] S. V. Vaseghi, "*Advanced Signal Processing and Digital Noise Reduction,*" Teubner-Wiley, 1996, ISBN 0-471-95875-1